# Designing the Interface of Transition Metal Phosphides for Electrocatalysis

David Ung

A dissertation

submitted in partial fulfillment of the

requirements for the degree of

Doctor of Philosophy

University of Washington

2020

Reading Committee:

Brandi M. Cossairt, Chair

Bo Zhang

Dianne J. Xiao

Program Authorized to Offer Degree:

Chemistry

University of Washington

## Abstract

Designing the Interface of Transition Metal Phosphides for Electrocatalysis

David Ung

Chair of the Supervisory Committee:

Associate Professor Brandi M. Cossairt

Department of Chemistry

Colloidally synthesized nanocrystals are a compelling class of materials for catalysis due to their high surface-area-to-volume ratios. The surface chemistry of nanocrystal catalysts is particularly important because of its impact on the electronic structure of the nanocrystal but also because it comprises the interface between the catalyst, substrate, solvent, and even electrolyte in the case of electrocatalysis. This dissertation focuses on how the interface between a nanocrystal catalyst and the substrate can be designed and modified to promote electrocatalytic activity.

Chapter 1 highlights the important role interfaces play in energy conversion and storage technologies and introduces key electrochemistry concepts for the remainder of the thesis. Chapter 2 describes how common surfactants impact the electrocatalytic activity of cobalt

phosphide (CoP) nanocrystals for the hydrogen evolution reaction (HER) in aqueous electrolyte solutions. Chapter 3 discusses the unintuitive differences in electrochemical behavior between nanocrystal catalyst films in aqueous versus non-aqueous solvents and examines the important role outer-sphere solvent interactions play in electrocatalytic activity of transition metal phosphides for HER.

# TABLE OF CONTENTS

# LIST OF FIGURES

# LIST OF TABLES

# ACKNOWLEDGEMENTS

Graduate school has been an incredibly challenging experience, as it should be. But what a privileged life it has been to be able to come to work and have my objective be to learn every day. As I near the end of my graduate school education, I find myself looking back at the people who have supported me and encouraged me in my life and I am incredibly grateful for them. This Ph.D. would not have been possible without them.

First and foremost among these people who have supported and encouraged me is my family. My parents are Cambodian refugees and have sacrificed a lot for me to pursue a Ph.D. They fled Cambodia with my older brother and settled down in Los Angeles, before having two more children. I imagine raising children is challenging enough without having to navigate a whole new country and culture. My parents are the most disciplined people I know and my childhood is filled with memories of them working incredibly late hours to provide for us. Over 30 years after my parents immigrated to the United States, they have raised three children. Between the three of us, there are three bachelors degrees, two masters degrees, and assuming this dissertation goes well, one Ph.D. I am proud to be their son and I hope they can look back at all they have sacrificed and feel that it has been worth it. Those who know me well know that I am incredibly close with my siblings. They have been my biggest supporters in graduate school and in life, and have taught me to be curious about the world. To this day, our relatives comment about how well we get along and how we're always talking to each other when we're together. They are kind and compassionate people and are my biggest role models to this day. My older

brother paved the way for my sister and me to receive the opportunities we've had, and I will always be thankful. My older sister was the key figure in my childhood who showed me how important it is to be polite and treat everyone with kindness. I am the spoiled youngest child and I hope to repay everyone in my family for all they've given me some day.

I was never particularly interested in scientific research growing up, but I was fortunate enough to stumble into a research position in Cliff Kubiak's lab during my time at UC San Diego. I had two incredible graduate student mentors, Candace Seu and Gabriele Canzi. Candace taught me everything I know about chemistry and about giving a good presentation. But through her example, she also taught me how to be a good mentor and an incredibly thoughtful friend. Our time together chatting in the lab, or at her dining table, or on bike rides in San Diego are among my favorite memories of my time in college. Gabe was my self-proclaimed life mentor who taught me that graduate school could be fun, and that maintaining hobbies was not only possible in graduate school but also critical to live a balanced life. The Kubiak lab was loud, chaotic, and sometimes messy, but they treated each other like family. The experience I had in that lab is what convinced me to pursue graduate school.

When I came to the University of Washington, I immediately knew I wanted to join the Cossairt lab because even though they were a relatively new lab, I could sense a similar energy to the Kubiak group. Over the years the lab has grown to become an incredibly fun and supportive environment. We care about the science and work hard, but we somehow manage to find a balance to stay happy. Critical to this supportive environment is an incredible advisor, Brandi Cossairt. I have struggled to find my place in graduate school, but thanks to Brandi's support I think I have managed to find my own success. She has been incredibly patient with me as I took the time to determine what I wanted to get out of the program and she has given me the

freedom to manage my own research without looking over my shoulder. That respect and trust is incredibly valuable to me and I cannot imagine a better advisor for my graduate school experience.

I have always found the lab to be a warm, welcoming environment that has been full of laughter and support over the years and it is incredible that the lab somehow manages to maintain its culture and personality even though it is constantly evolving. I am proud to have played a small role in cultivating the close-knit community over the years. The most important part of this dynamic is the people. Danielle, Ben, Mike, Dylan, and Betsy were the first members of the lab and I appreciate all they did. Danielle and I were the original two members of team electrochemistry, and I cannot imagine better company. The late night office chats talking about chemistry are among my favorite memories of graduate school. She has taught me a lot about chemistry, friendship, and FODMAPs. Ben was the student you could always go to for help, and I tried my best to emulate his generosity as I transitioned into a more senior student. Mike gave me incredible advice for choosing which lab to join when I first entered the program, and it is advice I continue to pass on to incoming students. Dylan was never shy about being himself and I respected his confidence. Betsy would always be willing to participate in a good joke in the office and I appreciate the laughs that we shared. Jenny and Coleman were in the second group of students and were the life of the party when I first joined. Jenny has eaten many delicious meals with me I thank her for keeping me company while I played stressful video games. She is often the extrovert to my introvert. Coleman was the source of the original social office. He was always warm and welcoming no matter who wanted to chat. I joined the lab in the third group of students, with Michael and Beth. Michael is one of the hardest workers I know and his loyalty to his friends and family is an inspiration. He and I worked in the same office for over five years,

sometimes sharing a fume hood. It is safe to say that he was a critical part of my graduate school experience. Beth and I had very similar experiences in the graduate program. I appreciate her commiseration and her company in our shared stubbornness to make it through. She often brought in baked goods that were always a pleasant surprise and could bring a small bit of happiness during stressful days. Andrew joined in the fourth group of students. I appreciate his ability to build (and sometimes 3D print) things to solve problems in lab. Max joined as a postdoc shortly after. He has been an incredible source of knowledge and a great role model for the lab. I can only hope to know as much as he does about chemistry and birdcalls. Cecilia and Ian were the fifth group of students. Cecilia has been an incredible friend since I first met her and I appreciate her trust and patience in me, even though I can be overbearing at times. She is one of the few people I know who regularly laughs until she cries, and her ability to smile and laugh through tough times is something I hope to implement more in my life. I look forward to not getting lost but instead going on adventures with her in the future. Ian was a late addition to the lab but immediately fit in. He is the best doppelganger I could ask for. I find it incredible how similar we are while somehow being complete opposites at the same time, and I appreciate his ability to make me laugh and to get me out of my comfort zone. Nayon, Tyler, and Madison were in the sixth group of students. Nayon is one of the most generous people I know and has been the person in the lab who is most likely to get me out of the house on a weekend. Her positive attitude while working incredibly hard is something I genuinely admire. And without her, I probably would have starved in graduate school. Tyler is one of the funniest people I've had the pleasure of meeting. His time in the lab has brought many laughs and he could regularly improve the mood of the lab singlehandedly. Madison has an incredible balance of charm, sass, and wit. I have always enjoyed our playful jokes towards each other while chatting in the office.

Florence and Forrest were the seventh group of students. Florence has been incredibly patient with me in the time I've known her. We often fight and nag each other but I am glad we both understand it comes from a good place. I am thankful for the trust she places in me and I believe that convincing her to join the lab was one my greatest achievements in graduate school. Forrest somehow manages to laugh and smile even when he is overwhelmed. His ability to keep chugging along is incredible and is something I can only hope to emulate. Ding-Yuan joined as postdoc shortly after. I enjoy his quiet demeanor while silently judging us in the office, while occasionally joining in to laugh with and at us. Ricardo and Micaela are the eighth and most recent batch of students. Ricardo is incredibly kind and thoughtful, and I think he will be a great addition to team electrochemistry. Micaela is somehow a mix between Ian and me. Her laugh brings a lot of energy into the lab and I appreciate her willingness to learn and play. Through all of these groups of graduate students and postdocs, I have also had the opportunity to work alongside some amazing undergraduate students. I was able to work particularly closely with Noush, who is not only an incredible student but also a great friend. His sense of humor is second to none and I am thankful that he came up with the tagline: "we get a lot done." Being able to meet and work with this group has been the greatest opportunity I have had in graduate school, and I would like to thank everyone for contributing to the positive lab culture and to my graduate school experience. I realize that I am not nearly as funny or as clever as I like to think I am, and I appreciate everyone humoring me over the years.

The lab has been a wonderful work environment but I have also had an excellent support network outside of the lab in Seattle. I am incredibly grateful for their ability to keep me balanced and for reminding me that there is more to life than research. Becky has been a regular picnic partner and I am thankful for all of the times she has reassured me while I had anxiety

about presentations. She is one of the most welcoming people I know and I am grateful for her invites to spend holidays with her family. Tim, Alex, Chris, Sterling, and Nate have made me feel incredibly cool by association. I never would have thought I would be a couple of degrees of separation from category 1 bike races, crazy house parties, art shows, or demolition derbies.

One of the sayings I've heard in graduate school is "only you can get yourself a Ph.D." This saying is meant to relay the idea that at the end of the day, the individual student needs to put in the work in order to achieve success. While this is true, I would not be in this position without the incredible support from the people I've mentioned above as well as many others. I am so grateful for everyone's help in getting me here today, and I hope that I have been able to give back a small fraction of the support I've been able to receive. It's a beautiful life.

# Chapter 1. Introduction

## 1.1 Surfaces of Colloidal Nanocrystals Define the Interface

Broadly defined, an interface is a surface that forms a common boundary between two things. The characteristics of this boundary are incredibly important in influencing how the two objects interact. For example, when working with dough while baking, the interface between the dough and the hands that knead it can impact how difficult it is to work with. If the interface is comprised of moist air, the dough is incredibly sticky and challenging to manage. But if there is a layer of flour or oil at the interface of the dough, the interaction becomes much more facile. Similarly, the interface between the ground and our feet can also have drastic effects. On an average day where the ground is dry, there is enough friction between the ground and our feet to be able to walk with little concern. However, if there is a thin layer of water or ice at the interface, walking can become much more treacherous.

While there are many macroscopic examples of interfaces impacting interactions between two things, there are many microscopic examples as well, especially in the world of energy conversion and storage. The presence of the solid-electrolyte interphase (SEI) between a battery electrode and the bulk electrolyte solution is a critical component to its functionality and greatly impacts its performance and energy capacity.[1,2] Similarly, the interface between two doped semiconductors forms a p-n junction, which is essential for charge separation and ultimately the conversion of solar energy to electricity in a solar photovoltaic device.[3] The field of energy conversion this dissertation focuses on is in artificial photosynthesis, where the overarching goal is to emulate the ability of plants to use solar energy to form new, energy-dense chemical bonds

to be used as a chemical fuel. However, the vast majority of fuel-forming reactions are not only thermodynamically uphill but also have large kinetic barriers associated with them (Figure 1.1).

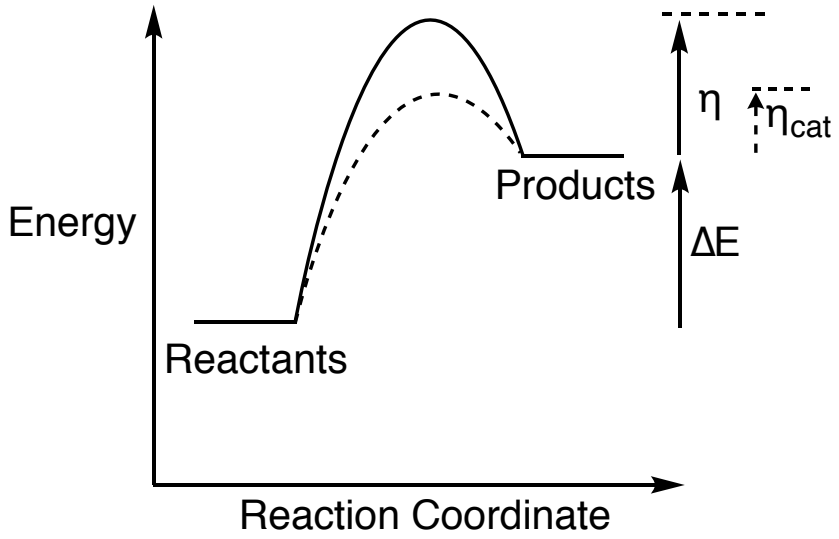


Figure 1.1. Reaction coordinate diagram illustrating the energy barriers associated with most fuel forming reactions, as well as defining overpotential with and without a catalyst.

Catalysts must be implemented to improve the kinetics of these fuel-forming reactions. The surface of a heterogeneous catalyst is extremely important because it is where the substrate can interact with the catalyst to do the relevant transformation (Figure 1.2). However, in a bulk material, there is poor atom efficiency for catalysis because the vast majority of the material is on the catalyst interior and therefore unable to interact with substrate at the surface. Because of this, there has been a large focus to develop nanomaterials for catalysis due to the improved surface-area-to-volume ratio as well as the additional synthetic levers of adjusting the size or shape of the nanocrystal, which can influence both the kinetics and thermodynamics of inner-sphere reactions.[4–6] However, the surfaces of nanomaterials are quite complex due to their high surface energies. The complexities of the interface between the catalytically active surface with

the bulk solution plays a large role in its overall reactivity. The work carried out as part of this dissertation explores how the properties of the interface between a nanocrystal catalyst, the substrate, and the bulk solution influences its catalytic activity for the hydrogen evolution reaction.

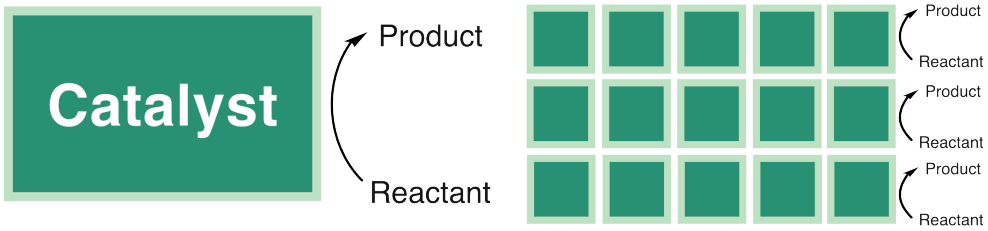


Figure 1.2. Illustration showing the intrinsically higher surface area with a nanoscale catalyst when compared to a bulk material.

## 1.2 Nanoparticles Have Complex Surfaces

The colloidal synthesis of nanocrystal catalysts is a promising approach for catalyst production due to its intrinsic scalability since it's performed in the solution phase. There has been a wide range of colloidal syntheses developed for a variety of nanomaterials, ranging from the production of semiconductor nanocrystals (quantum dots), to metallic nanoparticles, or even carbon-based systems.[7–11] This array of nanomaterials has been applied to many chemical transformations of interest, from electrocatalytic proton or $CO_2$ reduction, to hydrogenation chemistry, to even photocatalysis. However, regardless of the type of nanomaterial or its end application, all colloidally synthesized nanocrystals have complex interfaces due to the presence of surface ligands (Figure 1.3). These surface ligands are a necessity for the synthesis of colloidal nanocrystals because nanomaterials have intrinsically high surface energies and have a

thermodynamic driving force to grow larger, similar to water droplets. Surface ligands are used to stabilize the highly energetic surface, usually through a dative-type binding interaction. Furthermore, these surface ligands can participate in steric or electrostatic stabilization, allowing for stable colloidal suspensions by preventing the aggregation of the nanocrystals.[12–16] The most common surfactants used for colloidal syntheses are generally composed of a polar head group attached to a long chain hydrocarbon. The polar head group binds to the surface of the nanomaterial while the long chain hydrocarbon yields steric stabilization of the particles and allows for solubility in a wide range of organic solvents. Common surfactants used are long chain carboxylates, amines, phosphines, phosphonates, and thiolates.[12,14] These different surfactants can be utilized to yield particles of different sizes, shapes, and reactivity due to the variation in binding geometries and energetics. As an example, in the synthesis of cadmium selenide nanocrystals (CdSe), ligand interactions can play a large role in determining the resulting phase in a synthesis. Carboxylate ligands tend to stabilize the zinc blende structure of the nanocrystal while utilizing phosphonate ligands stabilizes the wurtzite structure. Wurtzite phase CdSe is amenable to anisotropic morphologies due to the high chemical potential along its (0001) axis.[17]

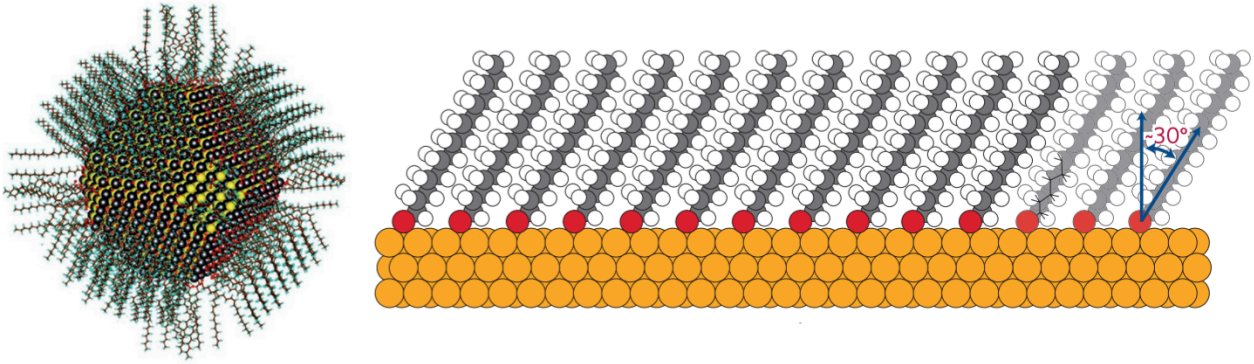


Figure 1.3. Illustration showing the nature of common surface ligands for colloidal nanocrystals with polar head groups and long aliphatic tails. Source: Boles, M. A.; Ling, D.; Hyeon, T.; Talapin, D. V. The Surface Science of Nanocrystals. *Nat. Mater.* **2016**, *15* (2), 141–153.

## 1.3 Motivation for the Electrocatalytic Production of Hydrogen

Many fuel-forming reactions require the movement of multiple protons and electrons (often at the same time) to form the relevant products (Figure 1.4). The hydrogen evolution reaction (HER) is the simplest multi-proton, multi-electron reaction and is simply the reduction of protons to form hydrogen gas. The work done in this dissertation focuses on the HER as a model system, with the goal that the conclusions formed by understanding how properties of the interface can affect HER can be applied to other interesting electrochemical transformations, such as the carbon dioxide reduction reaction ($CO_2RR$) or even nitrogen fixation. Coupling the movement of protons *with* electrons greatly reduces the associated thermodynamic barriers as seen in $CO_2RR$, where a single electron reduction of $CO_2$ has an extremely negative reduction potential. Understanding how the movement of protons and electrons can be manipulated by interfacial chemistry for HER will be key in developing new catalysts for these more complex transformations.

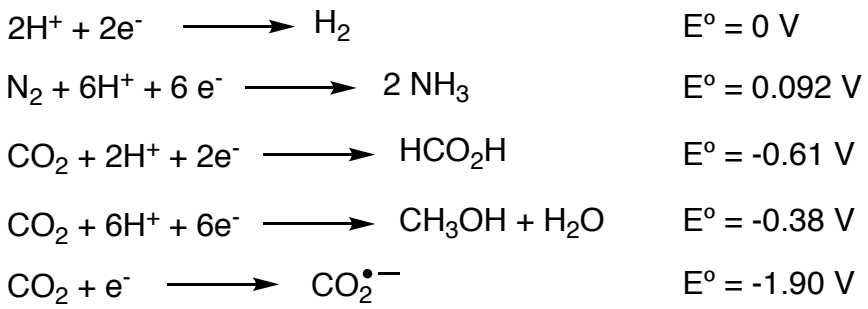


Figure 1.4. Reduction potentials of various fuel-forming PCET reactions. Potentials are referenced vs NHE.[18,19]

Hydrogen gas is also an important chemical commodity used for the production of ammonia and in petroleum refining.[20] The current state-of-the-art for the production of hydrogen gas is through the steam reforming of methane, which operates at extremely high temperatures (700-1000 ºC) and produces one mole of $CO_2$ for every 4 moles of $H_2$.[20] In order for hydrogen gas to be a feasible alternative fuel source to fossil fuels, its production needs to be energy efficient and carbon neutral. Water electrolysis with the use of an electrocatalyst may be a viable method of producing carbon-neutral hydrogen gas to be used both as a fuel source but also as a chemical commodity. The basics of electrochemistry and electrocatalysis will be briefly described in this introduction chapter.

## 1.4 Basics of Electrocatalytic HER

### 1.4.1 *Electrochemical cells*

A standard electrochemical cell is comprised of three electrodes: a working electrode, a counter electrode, and a reference electrode. For a heterogeneous electrocatalyst, the working electrode is where the catalyst is deposited in the form of a film. In most experiments, the potential at the working electrode is controlled via a potentiostat and the resulting current is measured. The counter electrode is used to complete the circuit by adopting whatever opposite

potential is necessary to compensate for the electrons transferred either to or from the working electrode. Finally, the reference electrode is used to reference the potential of the working electrode, allowing for accurate measurements. Depending on the experiment, the electrochemical cell may be filled with either an aqueous or non-aqueous electrolyte solution with the appropriate substrate. The electrolyte is a key component of the electrochemical cell and is required to improve the conductivity of the solution and prevents charge buildup at any of the electrodes. In the case of the HER, the substrate of interest is $H^+$.

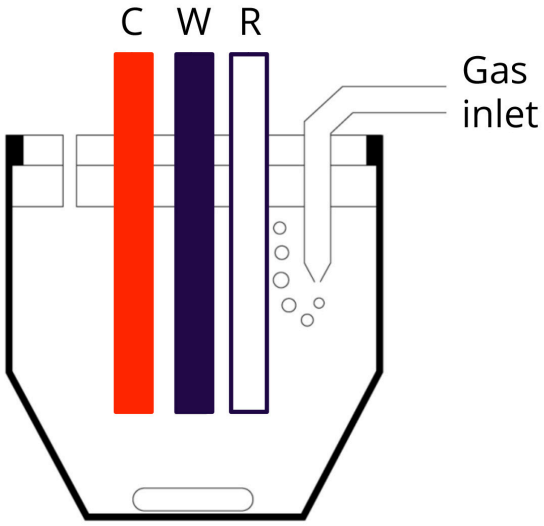


Figure 1.5. Illustration of the electrochemical cell.

It is important to note that proper experimental design is crucial to prevent contamination and convolution of electrochemical systems, especially given that electrochemical measurements can be extremely sensitive. The solvent and electrolyte must be highly pure to prevent contaminants from impeding measurements. Furthermore, electrode selection is critical. For example, platinum is often used as a counter electrode due to its inferred stability. However, platinum leaching in aqueous electrolyte can result in deposition of platinum on the working

electrode.[21] This deposited platinum can convolute the data, especially when studying HER due to its high activity for the reduction of protons. Similarly, high surface area carbon electrodes are common working electrodes and supports for heterogeneous catalysts. However, it is important to test that the intrinsic electrocatalytic activity of the bare working electrode is worse than the catalyst, otherwise the activity measured with a film of catalyst will not be representative of the deposited material.

### 1.4.2 *Understanding overpotential*

Fuel-forming reactions generally have large thermodynamic barriers due the goal of inputting and storing energy in the system through the formation of new chemical bonds. These thermodynamic barriers are *required* energy inputs into the system. However, these thermodynamic inputs are often coupled with high kinetic barriers as well. The extra energy input needed to overcome the kinetic barrier on top of the required thermodynamic input is defined as the overpotential (η), as seen in Figure 1.1. The goal of an electrocatalyst is to provide a new reaction pathway with lower kinetic barriers to decrease the overpotential and improve the overall rate of the reaction. For heterogeneous electrocatalysis in aqueous systems, platinum is considered the state-of-the-art for catalytic HER because the reduction of protons on platinum occurs near equilibrium.[22] Because of this, platinum is used as a reference for zero overpotential, referred to as the reversible hydrogen electrode (RHE). This is a system-specific reference potential where the potential of a platinum electrode under saturated $H_2$ is used as zero overpotential in the experiment's specific electrolyte conditions. The relevant figure of merit in the literature for heterogeneous aqueous electrocatalytic HER is the overpotential required for a current density of 10 mA/cm$^2$. This figure of merit was chosen due to the fact that it is the

expected current density required for an integrated solar-to-fuels device operating at 10% efficiency.[23]

Understanding overpotential in non-aqueous conditions can be more challenging, as the equilibrium potential of HER can change as a function of solvent and electrolyte conditions. Measuring the equilibrium potential for HER in specific non-aqueous systems can be done to obtain accurate overpotential measurements for catalyst benchmarking.[24,25] However, in this work we will focus on comparing catalysts that are modified in the same electrolyte conditions and will be referencing versus an internal standard (in the case of non-aqueous conditions, $Fc^{+/0}$).

## 1.5 Outlook

The colloidal synthesis of nanomaterials for catalysis is an important field of study because it allows for the scalable production of catalysts with high surface-area-to-volume ratios, which allows for high atom efficiency because the majority of the material is able to participate in the transformation of interest. The highly complex surface of a nanomaterial catalyst creates the interfacial boundary between the catalyst and substrate/bulk solution and can influence its overall activity. Electrochemical measurements are an important tool that allows us to measure the efficiency of various electrocatalysts by being able to study the rate of the reaction (current) as well as the overpotential. Most of the work in optimizing the interface between a nanomaterial catalyst and the substrate has been focused on removal of surface ligands to create a bare interface for improved activity. However, the work in this dissertation focuses on probing how the identity of the surface ligands on the interface can impact overall catalytic activity in order to develop design principles for transition metal phosphide electrocatalysts.

## 1.6 References


(1) Nandasiri, M. I.; Camacho-Forero, L. E.; Schwarz, A. M.; Shutthanandan, V.; Thevuthasan, S.; Balbuena, P. B.; Mueller, K. T.; Murugesan, V. In Situ Chemical Imaging of Solid-Electrolyte Interphase Layer Evolution in Li-S Batteries. *Chem. Mater.* **2017**, *29* (11), 4728–4737.

(2) Peled, E.; Menkin, S. Review—SEI: Past, Present and Future. *J. Electrochem. Soc.* **2017**, *164* (7), A1703–A1719.

(3) Shockley, W. The Theory of p-n Junctions in Semiconductors and p-n Junction Transistors. *Bell Syst. Tech. J.* **1949**, No. 28, 435–489.

(4) Cuenya, B. R. Synthesis and Catalytic Properties of Metal Nanoparticles: Size, Shape, Support, Composition, and Oxidation State Effects. *Thin Solid Films* **2010**, *518* (12), 3127–3150.

(5) Iablokov, V.; Beaumont, S. K.; Alayoglu, S.; Pushkarev, V. V; Specht, C.; Gao, J.; Alivisatos, A. P.; Kruse, N.; Somorjai, G. A. Size-Controlled Model Co Nanoparticle Catalysts for CO2 Hydrogenation: Synthesis, Characterization, and Catalytic Reactions. *Nano Lett.* **2012**, *12*, 3091–3096.

(6) Li, D.; Wang, C.; Strmcnik, D.; Tripković, D. V; Sun, X.; Kang, Y.; Chi, M.; Snyder, J.; van der Vliet, D.; Tsai, Y.; et al. Functional Links Between Pt Single Crystal Morphology and Nanoparticles with Different Size and Shape: The Oxygen Reduction Reaction Case. *Energy Environ. Sci.* **2014**.

(7) Cao, Z.; Kim, D.; Hong, D.; Yu, Y.; Xu, J.; Lin, S.; Wen, X.; Nichols, E. M.; Jeong, K.; Reimer, J. A.; et al. A Molecular Surface Functionalization Approach to Tuning Nanoparticle Electrocatalysts for Carbon Dioxide Reduction. *J. Am. Chem. Soc.* **2016**, jacs.6b02878.

(8) Chen, T.; Rodionov, V. O. Controllable Catalysis with Nanoparticles: Bimetallic Alloy Systems and Surface Adsorbates. *ACS Catal.* **2016**, No. 6, 4025–4033.

(9) Osterloh, F. E. Inorganic Nanostructures for Photoelectrochemical and Photocatalytic Water Splitting. *Chem. Soc. Rev.* **2013**, *42* (6), 2294–2320.

(10) Chen, X.; Shen, S.; Guo, L.; Mao, S. S. Semiconductor-Based Photocatalytic Hydrogen Generation. *Chem. Rev.* **2010**, 6503–6570.

(11) Razgoniaeva, N.; Moroz, P.; Lambright, S.; Zamkov, M. Photocatalytic Applications of Colloidal Heterostructured Nanocrystals: What's Next? *J. Phys. Chem. Lett.* **2015**, *6* (21), 4352–4359.

(12) Thanh, N. T. K.; Maclean, N.; Mahiddine, S. Mechanisms of Nucleation and Growth of Nanoparticles in Solution. *Chem. Rev.* **2014**, *114* (15), 7610–7630.

(13) Talapin, D. V.; Lee, J.-S.; Kovalenko, M. V.; Shevchenko, E. V. Prospects of Colloidal Nanocrystals for Electronic and Optoelectronic Applications. *Chem. Rev.* **2010**, *110*, 389–458.

(14) Boles, M. A.; Ling, D.; Hyeon, T.; Talapin, D. V. The Surface Science of Nanocrystals. *Nat. Mater.* **2016**, *15* (2), 141–153.

(15) Huang, W.; Hua, Q.; Cao, T. Influence and Removal of Capping Ligands on Catalytic Colloidal Nanoparticles. *Catal. Letters* **2014**, *144* (8), 1355–1369.

(16) Rossi, L. M.; Fiorio, J. L.; Garcia, M. A. S.; Ferraz, C. P. The Role and Fate of Capping Ligands in Colloidally Prepared Metal Nanoparticle Catalysts. *Dalt. Trans.* **2018**, *47* (17), 5889–5915.

(17) Enright, M. J.; Cossairt, B. M. Synthesis of Tailor-Made Colloidal Semiconductor Heterostructures. *Chem. Commun.* **2018**, *54* (52), 7109–7122.
(18) Kumar, B.; Llorente, M.; Froehlich, J.; Dang, T.; Sathrum, A.; Kubiak, C. P. Photochemical and Photoelectrochemical Reduction of CO2. *Annu. Rev. Phys. Chem.* **2012**, *63*, 541–569.
(19) Deng, J.; Iñiguez, J. A.; Liu, C. Electrocatalytic Nitrogen Reduction at Low Temperature. *Joule* **2018**, *2* (5), 846–856.
(20) Kothari, R.; Buddhi, D.; Sawhney, R. L. Comparison of Environmental and Economic Aspects of Various Hydrogen Production Methods. *Renew. Sustain. Energy Rev.* **2008**, *12* (2), 553–563.
(21) Dong, G.; Fang, M.; Wang, H.; Yip, S.; Cheung, H.-Y.; Wang, F.; Wong, C.-Y.; Chu, S. T.; Ho, J. C. Insight into the Electrochemical Activation of Carbon-Based Cathodes for Hydrogen Evolution Reaction. *J. Mater. Chem. A* **2015**, *3* (24), 13080–13086.
(22) Seh, Z. W.; Kibsgaard, J.; Dickens, C. F.; Chorkendorff, I.; Nørskov, J. K.; Jaramillo, T. F. Combining Theory and Experiment in Electrocatalysis: Insights into Materials Design. *Science (80-. ).* **2017**, *355* (6321), eaad4998.
(23) McCrory, C. C. L.; Jung, S.; Ferrer, I. M.; Chatman, S.; Peters, J. C.; Jaramillo, T. F. Benchmarking Hydrogen Evolving Reaction and Oxygen Evolving Reaction Electrocatalysts for Solar Water Splitting Devices. *J. Am. Chem. Soc.* **2015**, No. 137, 4347–4357.
(24) Appel, A. M.; Helm, M. L. Determining the Overpotential for a Molecular Electrocatalyst. *ACS Catal.* **2014**, *4* (2), 630–633.
(25) Roberts, J. A. S.; Bullock, R. M. Direct Determination of Equilibrium Potentials for Hydrogen Oxidation/Production by Open Circuit Potential Measurements in Acetonitrile. *Inorg. Chem.* **2013**, *52* (7), 3823–3835.

# Chapter 2. Effects of Surface Ligands on Cobalt Phosphide for the Hydrogen Evolution Reaction

Significant portions of the following chapter have previously been published.[1]

## 2.1 Introduction

### 2.1.1 *Scope of the study*

Colloidally synthesized nanocrystals are attractive for catalytic applications due to their synthetic tunability and solution processability. However, one trait all colloidally synthesized nanocrystals share regardless of their end application is the presence of ligands bound to the particle surface. These ligands are necessary to stabilize the high-energy surfaces and prevent aggregation of the particles in solution.

Throughout the literature, there has been a wide range of ligands used to stabilize colloidal nanocrystals, but among the most common are long chain amines, phosphines, phosphonates, thiolates, and carboxylates.[2–5] In most cases, the presence of these long chain, highly insulating surface ligands is considered a detriment to the nanocrystal's end application and they are removed through thermal or chemical treatments prior to use.[6–13] However, there are few fundamental studies examining the impact of the identity of surface ligands on catalysis.[13–16] In this chapter, we elucidate the mechanism in which traditional surface ligands impede catalysis by examining the role of ligands on cobalt phosphide nanocrystals for the electrocatalytic hydrogen evolution reaction as a model system.

### 2.1.2 *Transition metal phosphides*

Electrocatalysts must be used in order for the HER to be energetically feasible via water electrolysis. Platinum is the most widely used heterogeneous catalyst for the HER due to its high activity and stability in a range of operating conditions. However, because platinum is an incredibly scarce and expensive material (~$1000/oz), there has been a large push towards designing new catalysts from earth-abundant elements while retaining high activity. Recent work has shown that traditional hydrodesulfurization catalysts are often highly active at HER due to the requirement of similar surface-adsorbed hydrogen intermediates, as seen in Figure 2.1.[17–24] In particular, transition metal phosphides (TMPs) are emerging as one of the most promising materials to compete with platinum's reactivity. A wide range of non-noble transition metals have been used to synthesize their equivalent TMP nanomaterial, such as copper, cobalt, nickel, and iron. The colloidal syntheses of these materials have many synthetic levers to tune their size, morphology, and phosphorus content, which can yield different behaviors for different catalytic applications such as HER or hydrodeoxygenation catalysis, but also for use in Li-ion and Li-S batteries.[19,20,25,26] Our goal is to understand how the surfaces of nanoscale cobalt phosphide (CoP) alters their activity for HER, thereby developing design principles in order to reach the platinum level of activity.

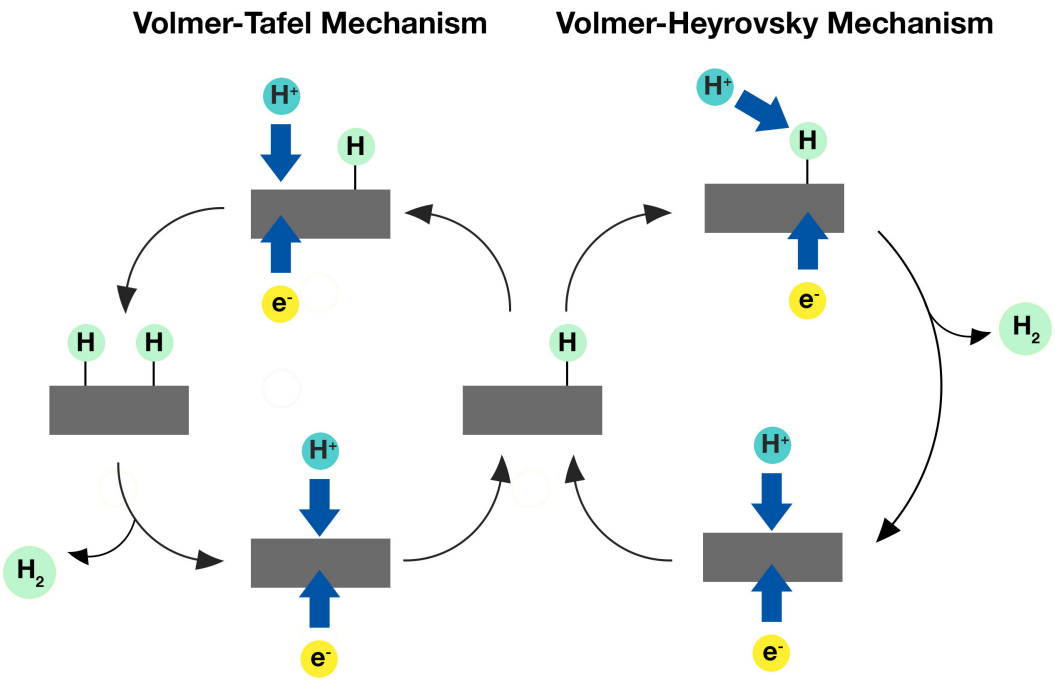


Figure 2.1. Both mechanisms for heterogeneous HER require the Volmer step, which yields a surface-adsorbed hydrogen intermediate which is also present in hydrodesulfurization catalytic mechanisms.

## 2.2 Experimental Method to Study a Variety of Surface Ligands

### 2.2.1 *The challenge of studying surface ligands on nanomaterials*

Studying the impact of different surface ligands on catalytic activity creates a unique challenge in the case of nanomaterials. Typically, surface ligands are used as a reagent in the synthesis of a nanomaterial and are present during the nucleation and growth of the particle. However, studying a series of surface ligands is not as simple as just changing what reagents are used in the reaction flask, because different surface ligands can alter the size, shape, and exposed facets of a nanocrystal (Figure 2.2).[2,27–29] This makes it difficult to draw meaningful conclusions

by studying a series of surfactants because the actual nanocrystal core itself is likely to be altered—too many variables have been changed. Our approach in this study is to generate a blank template by post-synthetically removing the surface ligands of colloidally synthesized cobalt phosphide, which we can re-ligate in order to keep the nanocrystal core constant.

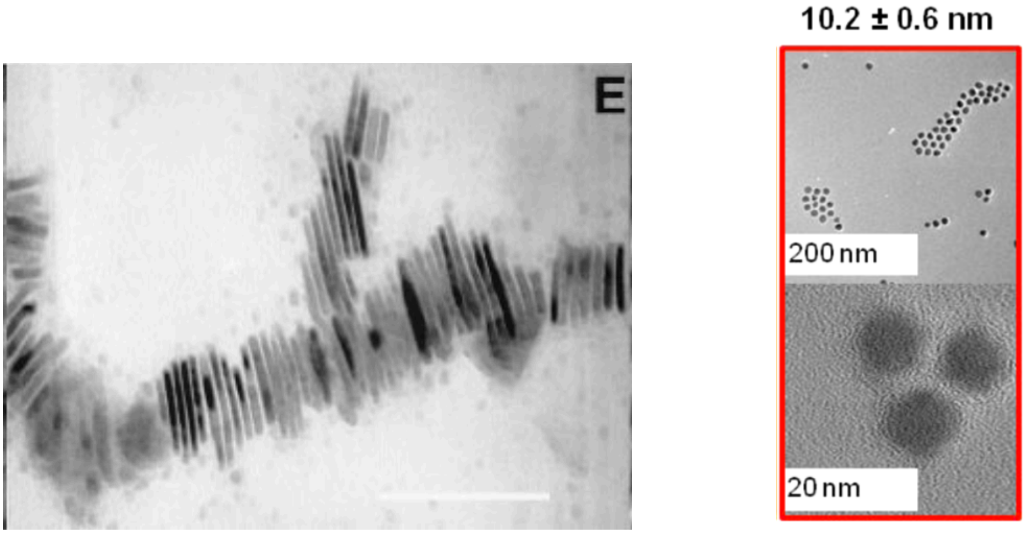


Figure 2.2. Cobalt nanocrystals synthesized with oleic acid and trioctylphosphine oxide yield ~100 nm nanorods. Using only oleic acid as a surfactant yields ~20 nm spherical nanoparticles. Source: (Left) Puntes, V. F.; Krishnan, K. M.; Alivisatos, A. P. Colloidal Nanocrystal Shape and Size Control: The Case of Cobalt. *Science* **2001**, *291* (5511), 2115–2117. (Right) Iablokov, V.; Beaumont, S. K.; Alayoglu, S.; Pushkarev, V. V; Specht, C.; Gao, J.; Alivisatos, A. P.; Kruse, N.; Somorjai, G. A. Size-Controlled Model Co Nanoparticle Catalysts for CO2 Hydrogenation: Synthesis, Characterization, and Catalytic Reactions. *Nano Lett.* **2012**, *12*, 3091–3096.

### 2.2.2 *Creating blank templates—ligand removal techniques*

The typical approach to removing surface ligands from a heterogeneous nanoparticle catalyst is through high temperature annealing. Essentially, the particles are exposed to elevated temperatures in order to burn the surface ligands off. This can be done under different

atmospheres such as air, argon, hydrogen, or vacuum in order to alter the surface chemistry of the nanocrystals. While this method has been used effectively to remove surface ligands and improve catalytic activity, it can alter the structure of the original nanocrystals and can also lead to particle sintering, which reduces the advantage of the high surface-area-to-volume ratio of nanomaterials have by limiting their catalytic efficiency by decreasing the number of active sites on a per mass basis.[7,10–12] Recent advancements in the field has shown a variety of chemical treatments for ligand removal, such as treatment with strong bases, alkylating agents, or strong Lewis acids.[9,30] However, these chemical treatments can have varying efficiency in surface ligand removal. Treatment with alkylating agents has been shown to produce surfaces as clean as thermal treatments but does not suffer from sintering or structure alteration. This dissertation will focus on the use of trialkyloxonium salts, specifically triethyloxonium tetrafluoroborate (Meerwein's reagent), for ligand removal because of its rapid reactivity at room temperature and its versatility on a wide range of materials and effectiveness as a homogeneous as well as heterogeneous reagent (Figure 2.3). Work done in our group has shown that treatment of $WSe_2$ nanomaterials with Meerwein's reagent effectively removes surface amine ligands and greatly improves electrocatalytic activity for HER.[31,32] This method allows us to compare *only* the surface ligands without impacting the base morphology of the original nanocrystal.

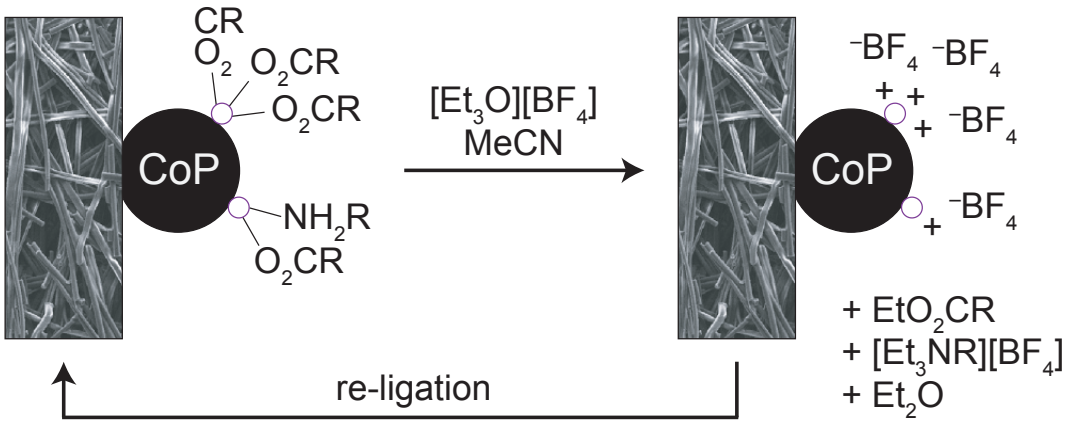


Figure 2.3. Scheme illustrating ligand stripping treatment with Meerwein's reagent, yielding an ester, ammonium salt, and diethyl ether.

In this chapter, as-synthesized CoP is drop casted onto carbon fiber electrodes for electrochemical characterization. Using a carbon fiber working electrode promotes even dispersion across the electrode as seen in the scanning electron microscopy image in Figure 2.4. Furthermore, the intrinsically high surface area of the carbon fiber support allows for large current densities.

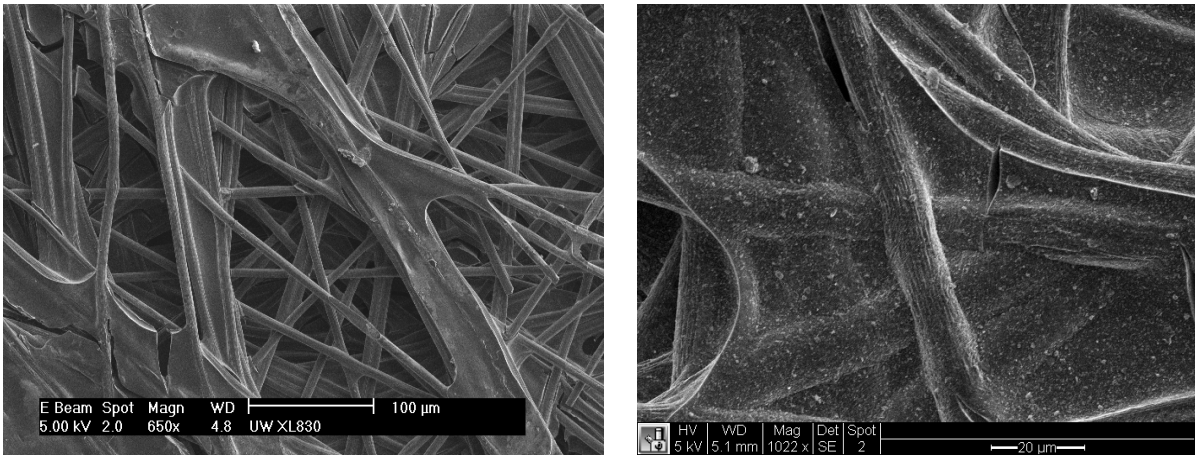


Figure 2.4. Scanning electron microscope image of a bare carbon fiber electrode (left) and a carbon fiber electrode with film of CoP drop casted on it.

This electrode can be dipped into a 0.1 M solution of trialkyloxonium tetrafluoroborate in 60 s increments to remove the native surface ligands to create a blank template. The Fourier-transform infrared (FTIR) spectrum shows the characteristic ligand stretching frequencies for the carboxylate and amine ligands on CoP pre- and post-stripping of the same sample. The peak intensities greatly diminish after treatment with Meerwein's reagent, illustrating that the vast majority of the surface ligands have been removed (Figure 2.5, left). We hypothesize that the remaining peak intensity is attributed to sub-surface layers of the CoP film that do not come in contact with the alkylating agent. This bare CoP electrode can then be treated with a solution of the surface ligand of interest (sodium salts in water for X-type ligands, amines in toluene for L-type ligands) to re-ligate the nanomaterial in order to compare the activity of CoP with a range of ligands. For example, when the bare CoP is treated with an aqueous solution of sodium oleate, the peak intensity of the C-H stretches grows back in, suggesting the presence of new surface ligands (Figure 2.5, right).

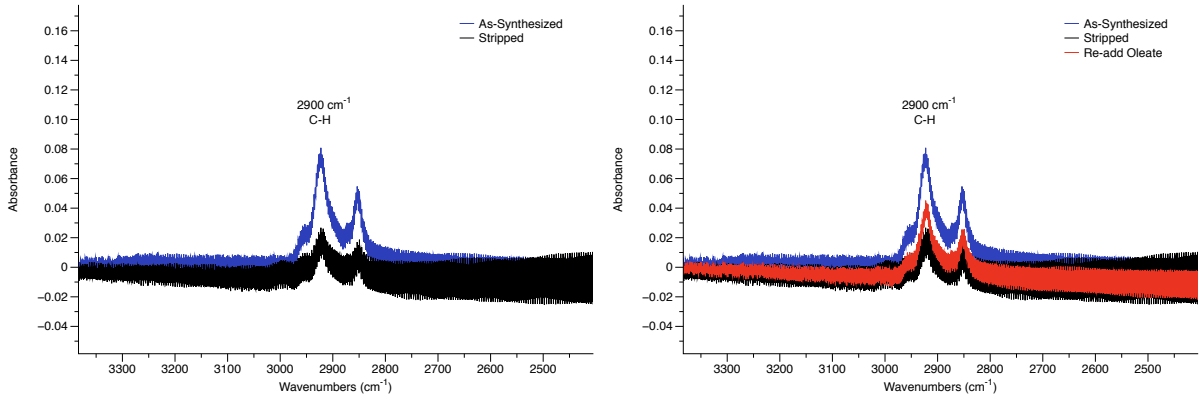


Figure 2.5. Fourier-transform infrared spectra of as-synthesized CoP, stripped, and re-ligated with oleate. The peaks at ~2900 $cm^{-1}$ represent the C-H stretches of the long chain hydrocarbons.

## 2.3 Comparing Surface Ligands: X-Type Carboxylates vs L-Type Amines

### 2.3.1 *Impact of ligand removal on overpotential*

Surface ligands are often removed on nanocrystal catalysts because they are considered to be a detriment to catalytic activity. When surface ligands are removed via thermal annealing, there is typically a resulting improvement in overpotential for electrocatalysis, attributed to either increasing the number or access to available active sites. This same improvement in overpotential can be seen in Figure 2.6, where treatment of an as-synthesized CoP electrode with 0.1 M solution of Meerwein's reagent leads to a ~500 mV improvement in overpotential for a current density of -10 mV/s.

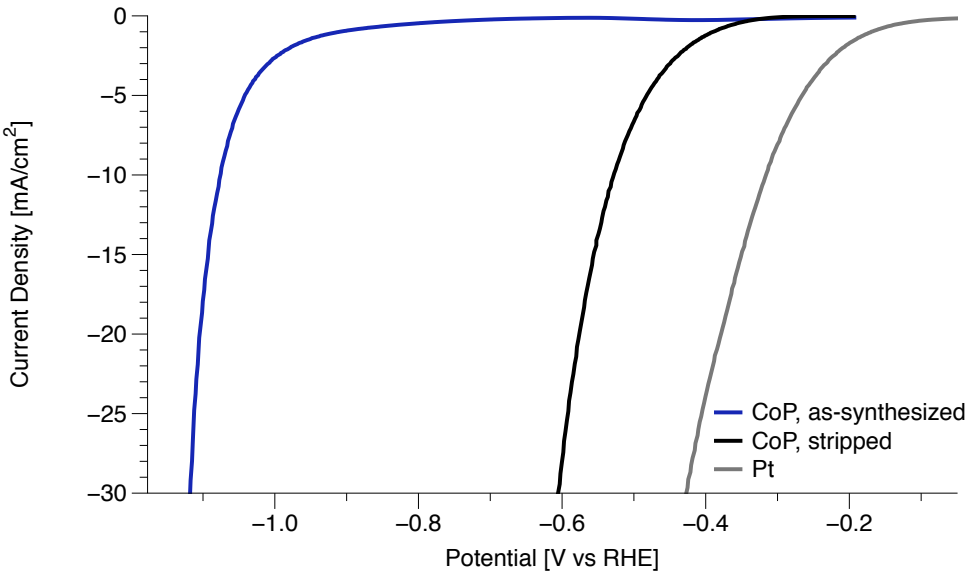


Figure 2.6. The stripped CoP decreases in overpotential by ~500 mV, getting closer to the Pt reactivity for HER.

### 2.3.2 *Comparing X-type carboxylates*

Carboxylates are anionic, X-type ligands and are among the most common surface ligands for colloidal syntheses of nanocrystals. Re-introducing oleate, one of the native surface ligands

for the CoP synthesis, to the stripped sample greatly increases the overpotential. The effect on overpotential of the carboxylate can be tuned by modifying the carbon chain length. As the chain length decreases, so does the overpotential (Figure 2.7). This is intuitive because the mechanism of HER requires the Volmer step, which forms a surface-adsorbed hydrogen as an intermediate (Figure 2.1). The increased steric demand of the carboxylate likely impedes the ability of the substrate to interact with the surface to form the necessary intermediate.

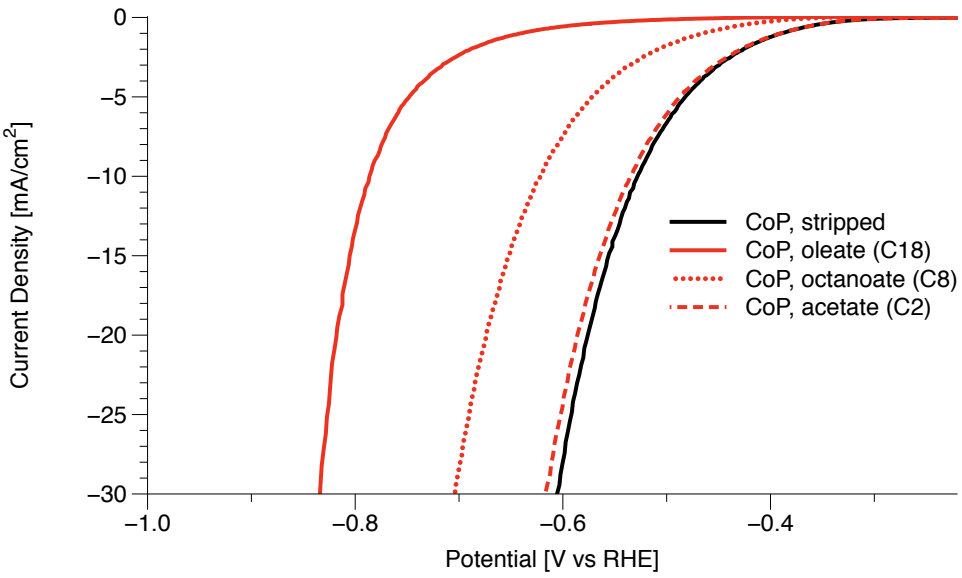


Figure 2.7. As the carboxylate chain length increases, so does the overpotential.

### 2.3.3 *Comparing L-type 1° amines*

Amines are neutral, L-type ligands and are another common type of surface ligand for traditional colloidal syntheses of nanocrystals and are often used as a solvent to promote high density on the surface. When a stripped CoP electrode is treated with a solution of oleylamine, there is a small increase in overpotential but much less when compared to the oleate, even though the particles have the same carbon chain. This suggests that the identity of the head group is a key component in the surface ligands' effect on electrocatalytic activity. Interestingly, there

is no significant variation in overpotential when adjusting the chain length of amines, unlike the carboxylates (Figure 2.8). This is due to the significant difference in ligand density when comparing an X-type carboxylate to an L-type amine. The anionic carboxylates likely have stronger binding to the surface of CoP when compared to the neutral L-type amines. Furthermore, these electrochemistry measurements are done in aqueous conditions where the neutral amines are likely to be protonated to form the equivalent ammonium. This reduction in the electron density on the head group would further weaken its binding affinity to the surface of CoP.

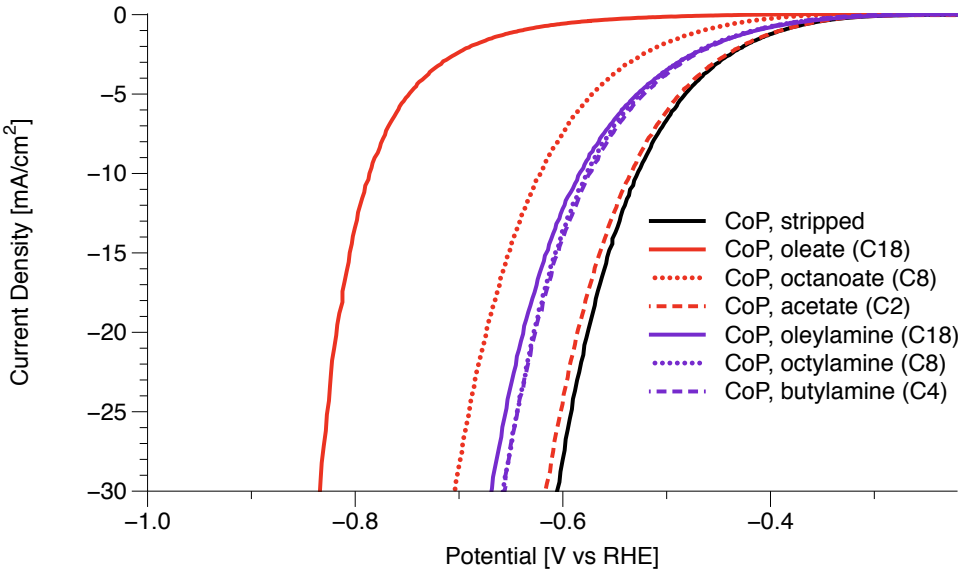


Figure 2.8. The 1° amine functionalized CoP have similar overpotentials, regardless of chain length. The equivalent carboxylate has a much higher overpotential than the amine.

### 2.3.4 *Estimating ligand density through electrochemically active surface area and thermogravimetric analysis*

The ligand density on CoP can be estimated by comparing the magnitude of the capacitive current at the open circuit potential as a function of scan rate to obtain estimates of the

electrochemically active surface area (ECSA).[6,33] The capacitive current is the charging current of an electrode, which measures the changes in the double layer as the potential is adjusted in a non-faradaic region of the cyclic voltammogram. If the electrode has more surface area to interact with the electrolyte solution, it essentially behaves as a larger capacitor, and a higher capacitive current can be measured (Figure 2.9). The stripped CoP sample should be able to form a large double layer across the surface of the electrode, which would yield the highest capacitive current and therefore ECSA. However, when surface ligands are added to the CoP, the effective surface area of the electrode that can interact with the electrolyte should decrease. The higher the ligand density on the surface of CoP, the lower the capacitive current and ECSA that will be measured.

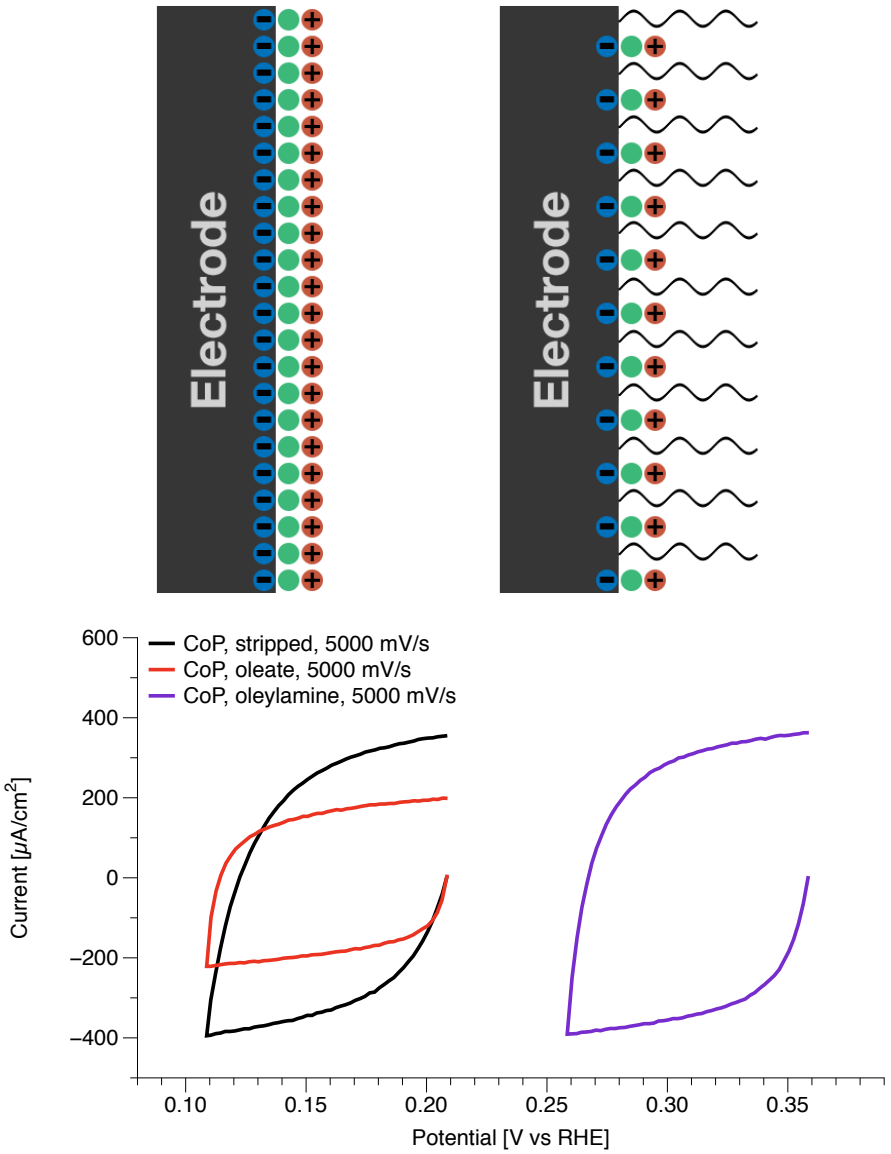


Figure 2.9. Surface ligands on the electrode prevent sections of the electrode from interacting with the electrolyte solution and disrupts the double layer, which decreases the capacitive current and ECSA.

In Figure 2.9 it can be seen that the capacitive currents of the stripped CoP and oleylamine-capped CoP are very similar in magnitude. However, the current of the oleate-capped CoP is significantly reduced, suggesting it has less surface area.

This is further supported when evaluating the ECSA values after performing scan rate dependence studies to approximate ECSA. As seen in Figure 2.10, there is a linear relationship between capacitive current and scan rate, the slope of which is defined as the double layer capacitance ($C_{DL}$). $C_{DL}$ can be used to calculate approximate values for ECSA by taking a ratio of the specific capacitance of the material in a given solution ($C_S$), as seen in Equation 2.1.[6]

$$ECSA = \frac{C_{DL}}{C_S} \qquad \text{Equation 2.1}$$

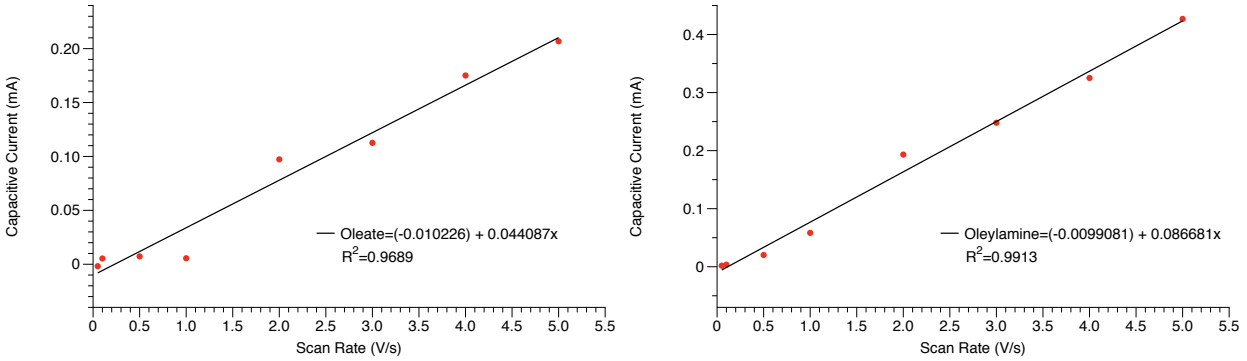


Figure 2.10. Scan rate dependence measurements of capacitive current have a linear relationship. The slopes of these lines are the double layer capacitance for the electrode with the ligated CoP. The remaining scan rate dependence traces can be seen in the experimental section.

The ECSA of the carboxylate and 1º amine-capped CoP are summarized in Table 2.1. The stripped CoP and the 1º amine-capped CoP all have similar ECSA values of ~2.6 $cm^2$, regardless of the chain length of the amine. On the other hand, the carboxylates have much lower ECSA values, ranging from 2.2 to 1.3 $cm^2$ with the longest carbon chain having the lowest surface area. The measured ECSA values support the hypothesis that the anionic carboxylates have higher ligand density on the surface of the nanocrystal due to their higher binding strengths.

Table 2.1. Summary of carboxylate and 1º amine-capped CoP

| Ligand | Overpotential (mV) | ECSA ($cm^2$) |
|---|---|---|
| Stripped | 532 | 2.6 |
| Oleate | 786 | 1.3 |
| Octanoate | 622 | 1.9 |
| Acetate | 535 | 2.2 |
| Oleylamine | 585 | 2.5 |
| Octylamine | 577 | 2.4 |
| Butylamine | 575 | 2.6 |

In order to further assess the relative ligand densities on CoP, thermogravimetric analysis (TGA) was used to compare the percent mass loss of oleate and oleylamine-capped CoP at equivalent loadings on a carbon fiber support. This analysis shows that there is a 2.4% mass loss on the oleate-capped CoP, while the oleylamine-capped CoP has a 1.9% mass loss (Figure 2.11). The masses of oleylamine and oleate differ by only 5%, so a variance of 21% between the two electrodes measured at the identical CoP loading confirms greater oleate versus oleylamine ligand density.

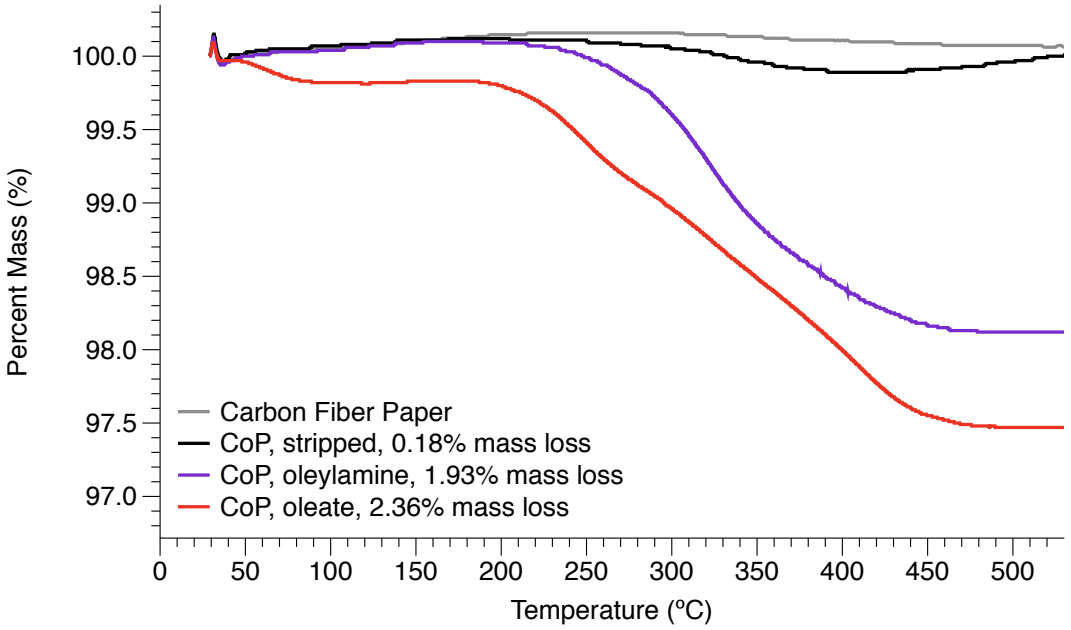


Figure 2.11. TGA of oleate and oleylamine-capped CoP illustrates differences in ligand density.

This difference in ligand density explains the change in overpotential when adjusting the carboxylate chain length but the consistent overpotentials when changing the 1º amine used. When the surface ligand of the NC is densely populated, an increase in carboxylate chain length provides sufficient steric bulk to inhibit substrate binding. However, when ligated with amines, there is a much smaller population of ligands on the surface, as seen by the ECSA and TGA measurements. Increasing the carbon chain on these amines does not significantly impede the solvated protons in solution from interacting with the surface since there is still a large amount of bare surface that is easily accessible. (Figure 2.12)

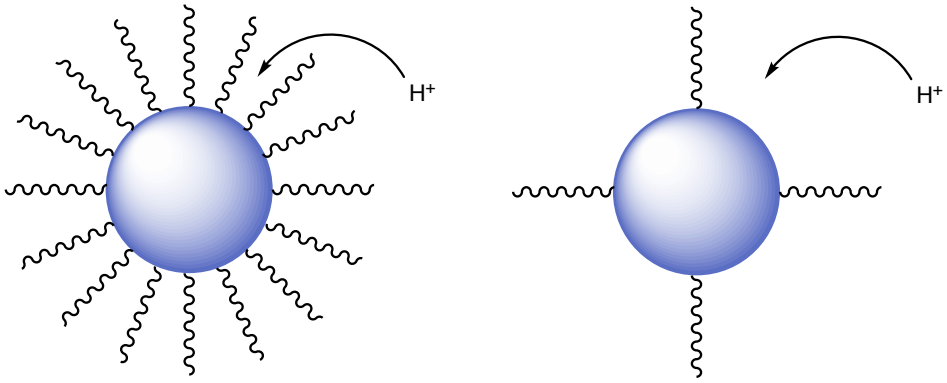


Figure 2.12. Altering chain length of surface ligands with low ligand density doesn't impede substrate from reaching the surface as much as a densely packed surface.

### 2.3.5 *Increasing effective amine ligand density by using 2° and 3° amines*

The effective ligand density of the amine surface ligands can be modified by using 2º and 3º amines. Shifting to 2º and 3º amines allows us to change the steric profile of the ligand by increasing the cone angle. With short chain amines, the cone angle can be adjusted ~50º by moving from 1º to 3º amines.[34] This is likely to be much more dramatic when moving towards long chain amines, such as octylamine. When dioctylamine and trioctylamine-capped CoP are measured, the overpotential increases compared to the 1º octylamine. This is also seen in the ECSA, where both the 2º and 3º amine-capped samples have lower ECSA values (Figure 2.13)

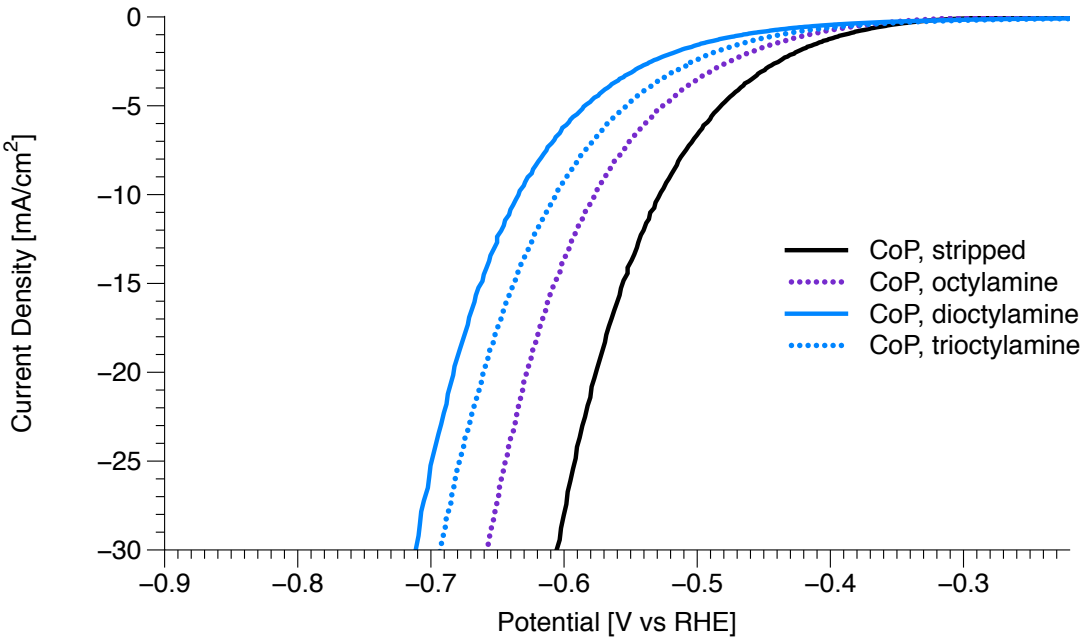


Figure 2.13. Changing the steric profile of the amines by increasing the cone angle increases the overpotential.

## 2.4 How Do Surface Ligands Impede Catalysis?

There are two common mechanisms proposed for how surface ligands can impede catalysis. The first is poisoning the active site through competitive binding (Figure 2.14). An example of this can be seen in $CO_2$RR with Ni(cyclam) electrocatalysts. Ni(cyclam) is active for $CO_2$RR to form CO. However, the catalyst is susceptible to self-poisoning as the reaction proceeds because the CO formed can strongly bind to the metal center to form a metal carbonyl species that is unable to activate new substrate molecules.[35] The second mechanism that is commonly invoked is that the steric profile of the surface ligands and its impact on chemical properties of the interface, such as polarity, inhibits substrate access to the catalytically active surface (Figure 2.12). If the first mechanism were operating, we would expect that all of the carboxylates tested, regardless of their chain length, would have similar activity since they have the same binding

head group. Or alternatively, acetate could have the worst activity because it has the smallest steric profile and would be able to coordinate to the active site to the largest extent.

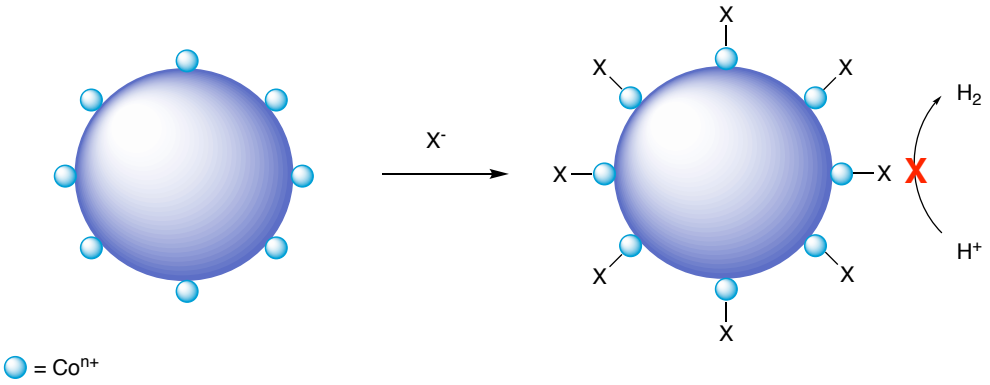


Figure 2.14. Impeding catalysis by poisoning active sites would occupy the available active sites.

However, the result we observe is that the longest chain carboxylates have the highest overpotential, and the shortest chain has the lowest. This suggests that the surface ligands are not poisoning the active sites, but rather create a steric barrier for the substrate to reach the catalytically active surface. This is further supported when observing the clear monotonic relationship between overpotential and ECSA, which shows that as the ECSA decreases, so does the activity (Figure 2.15, Table 2.2).

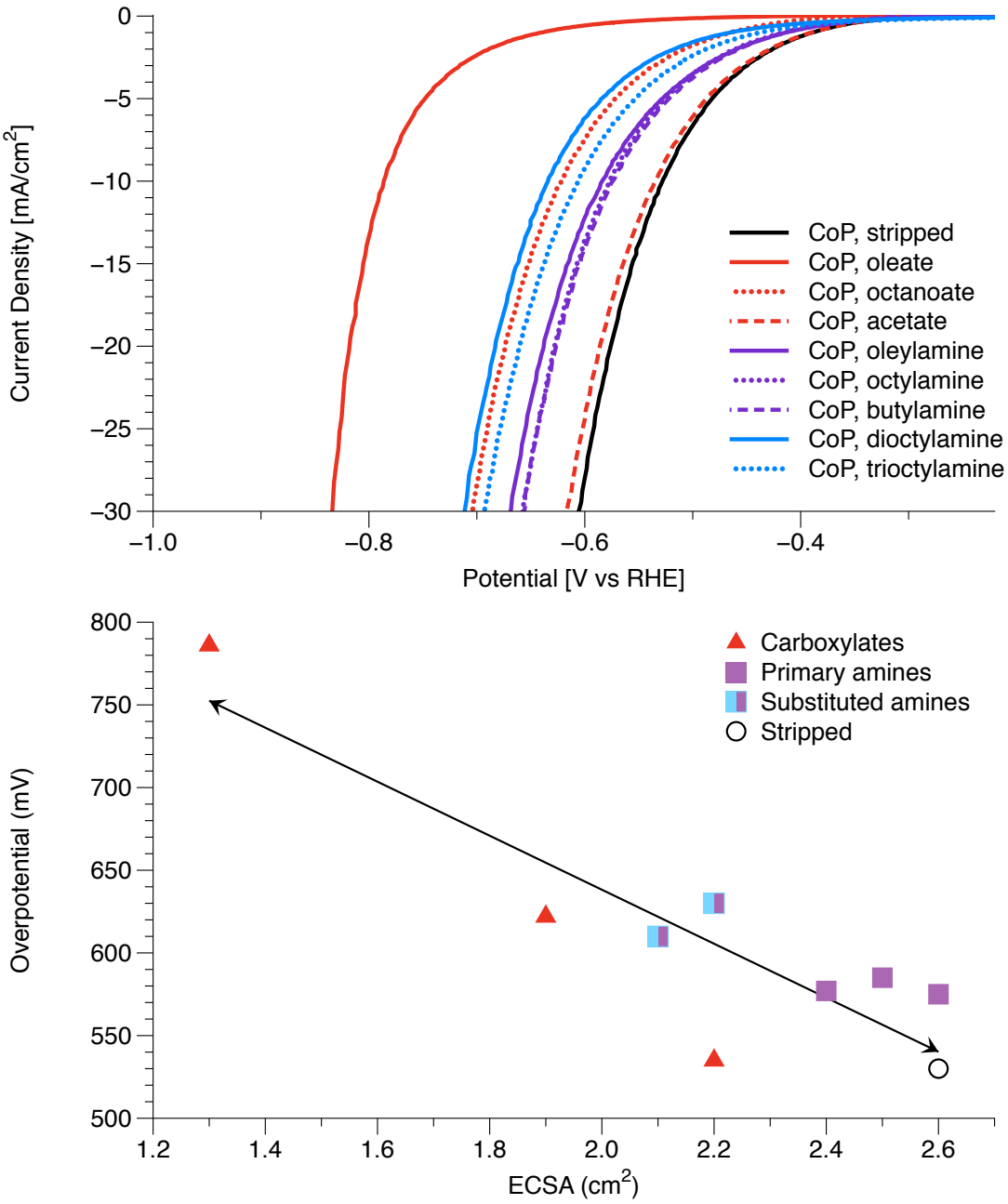


Figure 2.15. LSVs of all surface ligands used in this study (top). Plot of overpotential versus ECSA, which shows a negative monotonic relationship (bottom). As the ECSA of the CoP increases, so does the activity.

Table 2.2. Overpotential and ECSA measurements of the functionalized CoP films

| Ligand | Overpotential (mV) | ECSA ($cm^2$) |
|---|---|---|
| Stripped | 532 | 2.6 |
| Oleate | 786 | 1.3 |
| Octanoate | 622 | 1.9 |
| Acetate | 535 | 2.2 |
| Oleylamine | 585 | 2.5 |
| Octylamine | 577 | 2.4 |
| Butylamine | 575 | 2.6 |
| Dioctylamine | 630 | 2.2 |
| Trioctylamine | 610 | 2.1 |

## 2.5 The Importance of the Electrode-Electrolyte Interface

A rational argument against the conclusion that the surface ligands create a steric barrier that inhibits substrate from reaching the catalytically active surface is the fact that in the case of HER, the substrate are protons, which are extremely small. However, while protons are small and may not be inhibited by changes in the ligand shell, it is important to recognize that there are more factors operating in electrocatalysis than just the catalyst and the substrate. Electrocatalytic systems can be quite complex, with the catalyst film, substrate, electrolyte, and solvent all playing major roles in overall activity.[36–38] The aliphatic ligands create a steric barrier but also generate a hydrophobic interface that prevents both the substrate ($H^+/H_2O$) and electrolyte ($Na^+$, $SO_4^{2-}$) from accessing the surface of the CoP. This hydrophobic interface can be visualized with contact angle measurements (Figure 2.16), in which we observe that the wetting of a film of stripped CoP is much more favorable than the as-synthesized CoP capped by its native surface ligands (nonanoate, oleate, oleylamine).

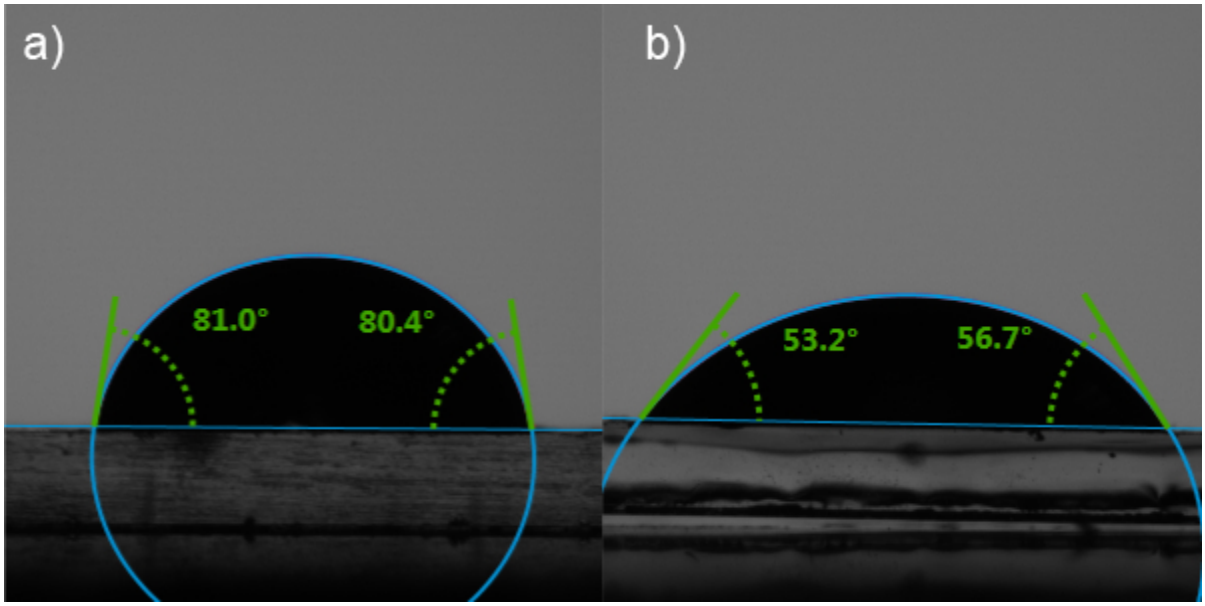


Figure 2.16. Contact angle measurements of an as-synthesized CoP film (a) and stripped CoP film (b) shows improved hydrophilicity of the film after removal of surface ligands.

## 2.6 Conclusions

In conclusion, we have examined the impact of surface ligands on the ability of CoP to catalyze the HER. Carboxylate and amine functionalized CoP have higher overpotentials than a bare nanocrystal. However, carboxylate-capped CoP has a higher overpotential than the equivalent amine. Furthermore, the overpotential of a carboxylate functionalized CoP can be increased by increasing the carbon chain length. This is due to an increase in steric bulk and hydrophobicity, which is supported by differences in the measured values of ECSA and the high contact angle of a film of ligated CoP. Conversely, the overpotential of the 1º amine-capped CoP is largely independent of chain length. This can be explained by the low ligand density when using amine ligands due to the relatively weaker binding of these neutral L-type ligands

compared to the anionic X-type carboxylates. Furthermore, these studies are performed in aqueous conditions, where a large fraction of the neutral L-type amines are likely protonated to form the equivalent ammonium, which would further reduce its binding affinity. These results illustrate that surface ligands on CoP for HER impede catalysis by inhibiting access to surface sites rather than poisoning the active sites, and suggests that catalysis does not occur on the excess cation on the surface, which is the site of carboxylate coordination. These results suggest that it may be possible to design a synthesis that uses surfactants that lead to colloidally stable NCs with similar or even improved activities when compared to a bare or annealed NCs. These results also show the critical role the electrode-electrolyte interface plays in electrocatalytic activity, which will be further explored in chapter 3.

## 2.7 Experimental

### 2.7.1 *Materials*

Dicobalt octacarbonyl (stabilized with 1-5% hexanes, $Co_2(CO)_8$, Strem, stored in glovebox), trioctylphosphine (TOP, Sigma-Aldrich, stored in glovebox), 2-propanol (anhydrous, 99.5%, Sigma-Aldrich, stored in glovebox), triethyloxonoium tetrafluoroborate (≥97.0%, Meerwein's reagent, Sigma-Aldrich, stored in glovebox), acetonitrile (anhydrous, 99.8%, MeCN, Sigma-Aldrich, stored in glovebox), octylamine (99%, Sigma-Aldrich), di-n-octylamine (97%, Acros), trioctylamine (98%, Sigma-Aldrich), n-butylamine (99+%, Acros), sodium oleate (>97%, TCI), sodium octanoate (≥99%, Sigma-Aldrich), sodium acetate (anhydrous, certified ACS, Fisher), nonanoic acid (≥97%, Sigma-Aldrich), oleic acid (technical grade, 90%, Sigma-Aldrich), toluene (HPLC grade, Fisher), 3-mercaptopropyltrimethoxysilane (MPTS, Sigma-Aldrich), and sodium sulfate ($Na_2SO_4$, ≥99.0%, anhydrous, Sigma-Aldrich) were used as received unless otherwise noted. 1-octadecene (1-ODE, technical grade, 70%, Sigma-Aldrich) and oleylamine (technical

grade, 90%) were dried over $CaH_2$, distilled, and stored over 4 Å molecular sieves in a nitrogen-filled glovebox. 18 MΩ Millipore water was collected from an EMD Millipore water purification system.

### 2.7.2 *Synthesis of ε-cobalt nanoparticles*

All glassware was dried in a 160 ºC oven overnight prior to use. All reactions, unless otherwise noted, were run under an inert atmosphere of nitrogen using a glovebox or using standard Schlenk techniques. Synthesis was adapted from Schaak *et al*.[24] 1-octadecene (50 mL, 156.6 mmol), oleylamine (30 mL, 91 mmol), nonanoic acid (10 mL, 56.5 mmol) were added to a 500 mL 3-neck flask equipped with a thermowell, condenser, and septum and was degassed at 120 ºC for 1 hour. In the glovebox, $Co_2(CO)_8$ (500 mg, 1.46 mmol) was suspended in 25 mL 1-octadecene. The reaction flask was heated to 230 ºC under $N_2$ and the $Co_2(CO)_8$ was slowly injected via syringe yielding a black solution. The reaction mixture was heated for 10 minutes and 10 mL of oleic acid was injected via syringe. The reaction mixture was heated for an additional 10 minutes and then removed from the heating mantle to cool. The resulting cobalt nanoparticles were purified in a glovebox by washing with isopropyl alcohol followed by centrifugation at 11000 rpm for 10 min. The cobalt nanoparticles were then resuspended in toluene and washed with additional isopropyl alcohol and centrifuged an additional two times. The resulting black solid was suspended in 10 mL of trioctylphosphine (21.5 mmol) in a glovebox, for conversion to CoP.

### 2.7.3 *Synthesis of cobalt phosphide nanoparticles*

1-octadecene (25 mL, 78.3 mmol), oleylamine (25 mL, 76 mmol), and trioctylphosphine (25 mL, 56 mmol) were added to a 500 mL 3-neck flask equipped with a thermowell, condenser, and

septum and was degassed at 120 ºC for 1 hour. The reaction flask was heated to 320 ºC under $N_2$ and the cobalt nanoparticle solution in trioctylphosphine was slowly injected via syringe. The resulting mixture was heated at 320 ºC for 1 hour. The reaction flask was removed from the heating mantle to cool. The resulting cobalt phosphide nanoparticles were purified in a glovebox by washing with isopropyl alcohol followed by centrifugation at 11000 rpm for 10 mins. The particles were then resuspended in toluene and washed with isopropyl alcohol and centrifuged an additional two times. The resulting black solid was suspended in toluene to prepare a 10 mg/mL solution for later use. 15 to 30 nm CoP was synthesized as seen in the powder x-ray diffraction (XRD) measurement and transmission electron microscopy (TEM) images, (Figure 2.17).

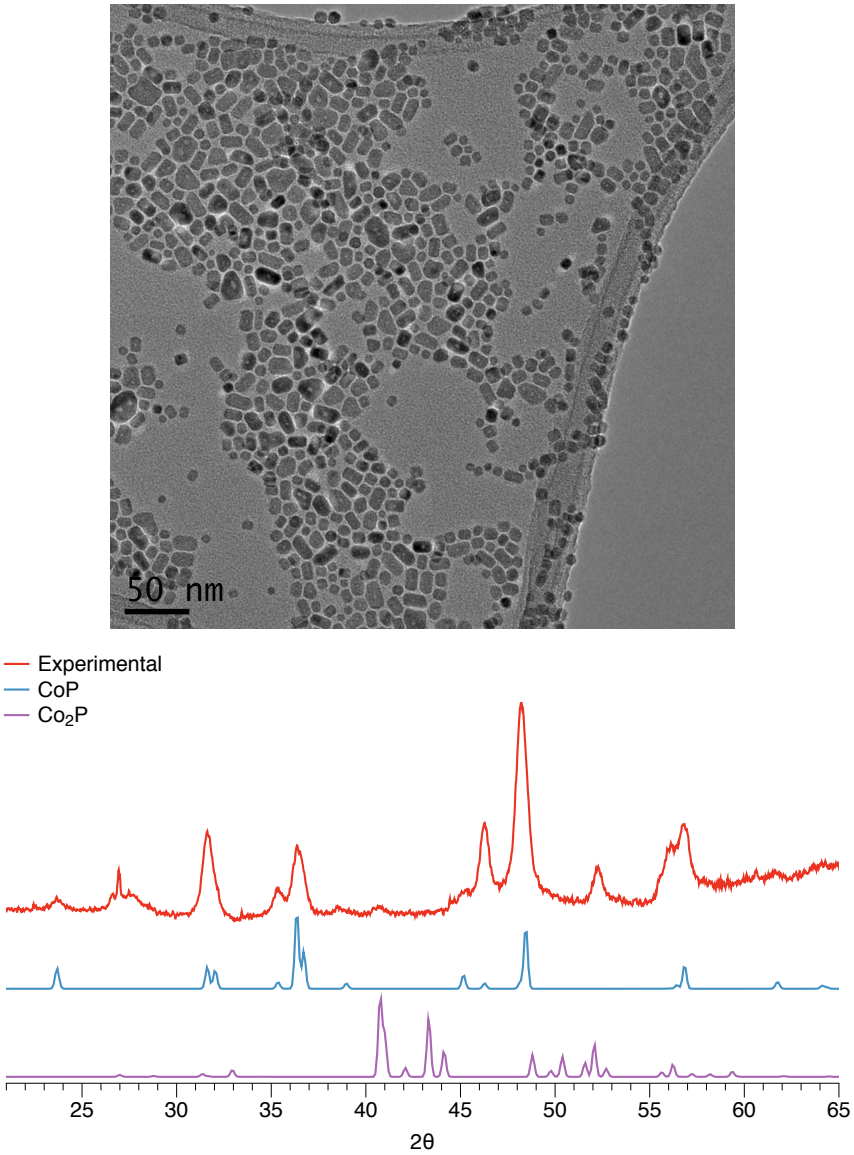


Figure 2.17. TEM of as-synthesized CoP (top) and powder XRD showing that CoP is the major product of the synthesis (bottom).

### 2.7.4 *Electrochemical characterization*

Electrochemical measurements were conducted in a custom four-neck cell fitted with a graphite rod counter electrode separated in a fritted compartment, a $Ag/Ag_2SO_4$ reference electrode separated by a Vycor frit, and a carbon fiber working electrode. The carbon fiber

working electrodes were fabricated from carbon fiber paper (Fuel Cell Store, Spectracarb 2050A 0850). The carbon fiber paper was cut into 1 cm x 3 cm rectangles and a copper wire was attached with a conductive silver epoxy to the electrode material. After curing, the copper wire and silver epoxy were covered with gel epoxy to create a 1 cm x 1 cm working area on the electrode. The backside of the 1 cm x 1 cm working area of the electrode was not covered due to the porosity of the material and epoxy being able to leak onto both sides. The CoP samples were suspended in toluene in a glovebox and drop casted in 20 μL aliquots onto the working electrodes for electrochemical measurements. The working electrodes were transferred to gas-tight headspace vials with magnetic caps and septa and were brought into a Bel-Art Techni-Dome glove chamber for electrochemical measurements.

All electrochemical measurements were performed with a Gamry Interface 1000 in a Bel-Art Techni-Dome glove chamber flushed with Ar. The electrolyte solution was 0.5 M $Na_2SO_4$ in 18 MΩ Millipore water and was sparged with Ar before use. The solutions of Meerwein's reagent were prepared in acetonitrile, carboxylates were prepared in 18 MΩ Millipore water, and amines were prepared in toluene. When stripping off surface ligands, the electrode was removed from the cell, rinsed with copious amounts of 18 MΩ Millipore water, rinsed with acetonitrile, dipped in a vial of 0.1 M Meerwein's reagent in 60 s increments, and then rinsed with acetonitrile and water before reinsertion into the cell and tested with linear sweep voltammetry. The process was repeated until the trace from the LSV stabilized. The re-ligation steps with carboxylates were performed in a similar manner but were only rinsed with the 18 MΩ Millipore water. The re-ligation steps with toluene required a rinse with water, acetonitrile, and then toluene before dipping the electrode in the amine solution, and then the electrode was rinsed in the reverse order before reinsertion into the cell to remove any residual amine and toluene. The

same electrode/sample is re-used for multiple ligands to minimize variations in sample deposition and loading. Linear sweep voltammograms were performed at a scan rate of 5 mV/s. All measurements in this study were referenced versus the reversible hydrogen electrode (RHE). RHE was measured using a platinum coil electrode in 0.5 M $H_2SO_4$ saturated with $H_2$. Potentials were converted using the following Equation 2.2.

$$E_{RHE} = E_{Ag/Ag2SO4} + 0.059(pH) + E^0_{Ag/Ag2SO4} \quad \text{Equation 2.2}$$

The cyclic voltammograms performed to measure the electrochemically active surface area (ECSA) were taken in an 100 mV range around the open circuit potential. The ECSA was calculated using the following equation: $ECSA = \frac{C_{DL}}{C_S}$. The average of the capacitive current window at multiple scan rates were used to calculate $C_{DL}$. The average general capacitance used was $C_s$=0.035 mF/cm$^2$.[6,39] The potential versus scan rate plots can be seen below.

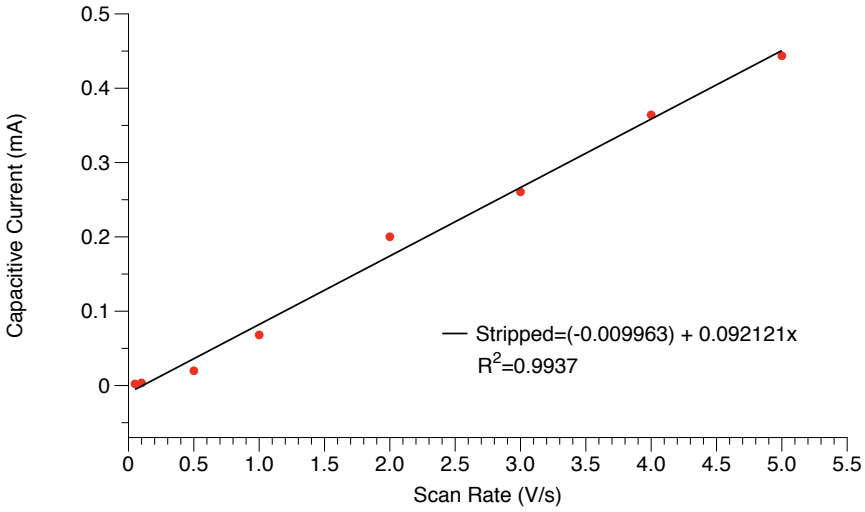
Capacitive Current (mA)
0.5
0.4
0.3
0.2
0.1
0
0
0.5
1.0
1.5
2.0
2.5
3.0
3.5
4.0
4.5
5.0
5.5
Scan Rate (V/s)
Stripped=(-0.009963) + 0.092121x
R2=0.9937

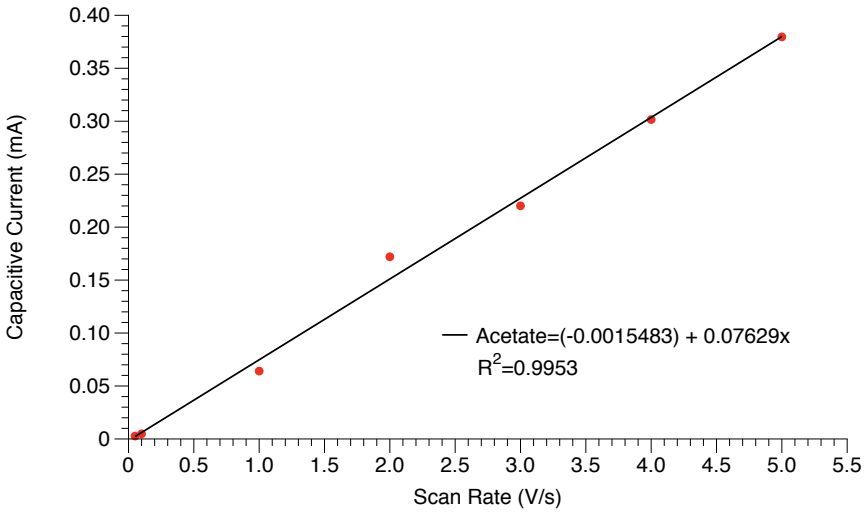
Capacitive Current (mA)
0.40
0.35
0.30
0.25
0.20
0.15
0.10
0.05
0
0
0.5
1.0
1.5
2.0
2.5
3.0
3.5
4.0
4.5
5.0
5.5
Scan Rate (V/s)
Acetate=(-0.0015483) + 0.07629x
R2=0.9953

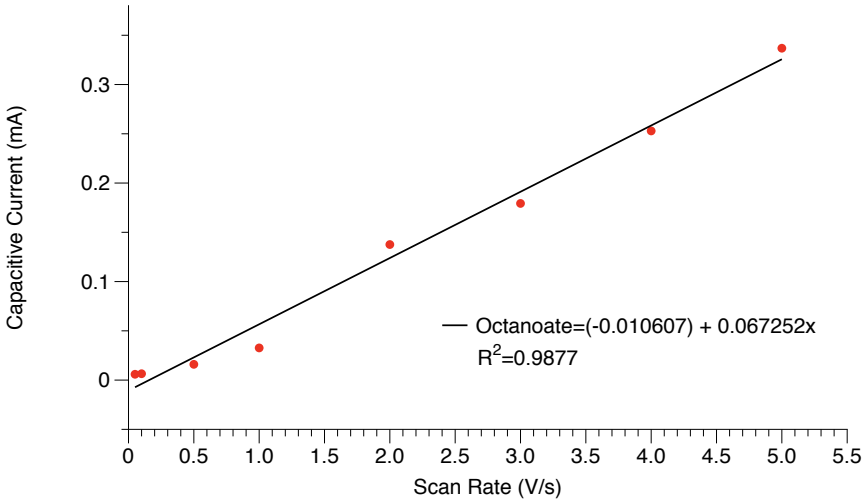
Capacitive Current (mA)
0.3
0.2
0.1
0
0
0.5
1.0
1.5
2.0
2.5
3.0
3.5
4.0
4.5
5.0
5.5
Scan Rate (V/s)
Octanoate=(-0.010607) + 0.067252x
R2=0.9877

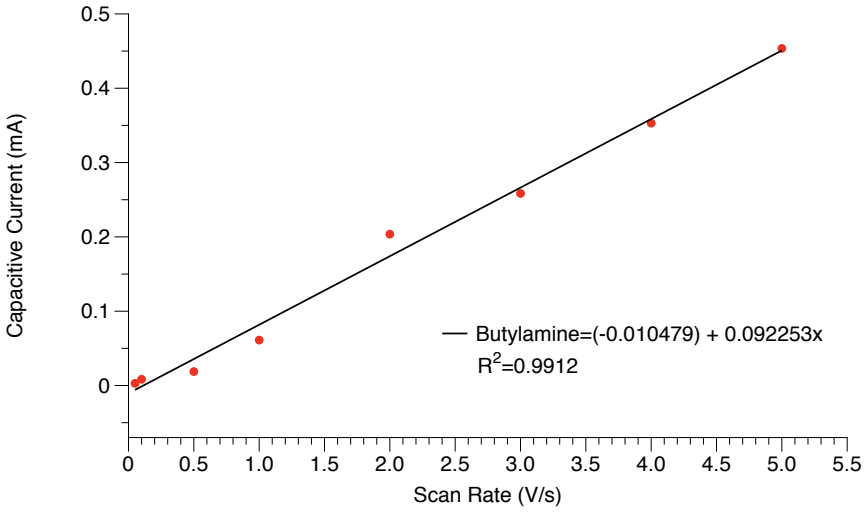
Capacitive Current (mA)
0.5
0.4
0.3
0.2
0.1
0
0
0.5
1.0
1.5
2.0
2.5
3.0
3.5
4.0
4.5
5.0
5.5
Scan Rate (V/s)
Butylamine=(-0.010479) + 0.092253x
R2=0.9912

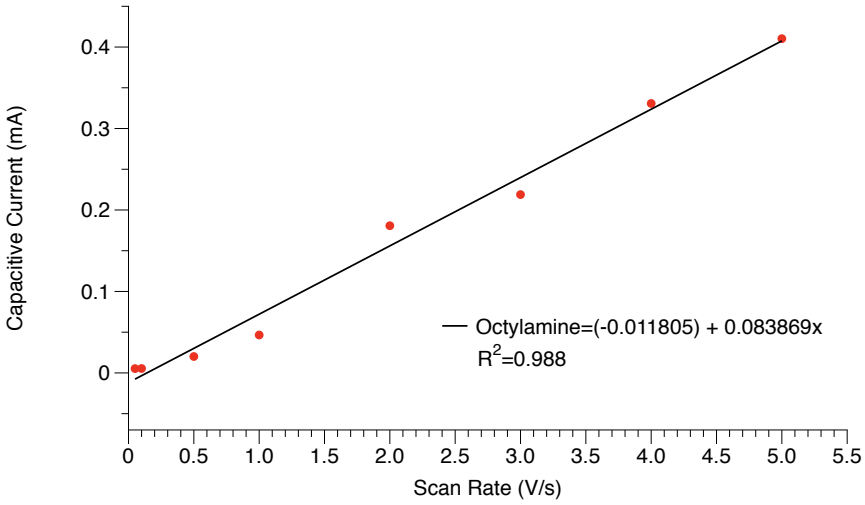
Capacitive Current (mA)
0.4
0.3
0.2
0.1
0
0
0.5
1.0
1.5
2.0
2.5
3.0
3.5
4.0
4.5
5.0
5.5
Scan Rate (V/s)
Octylamine=(-0.011805) + 0.083869x
R2=0.988

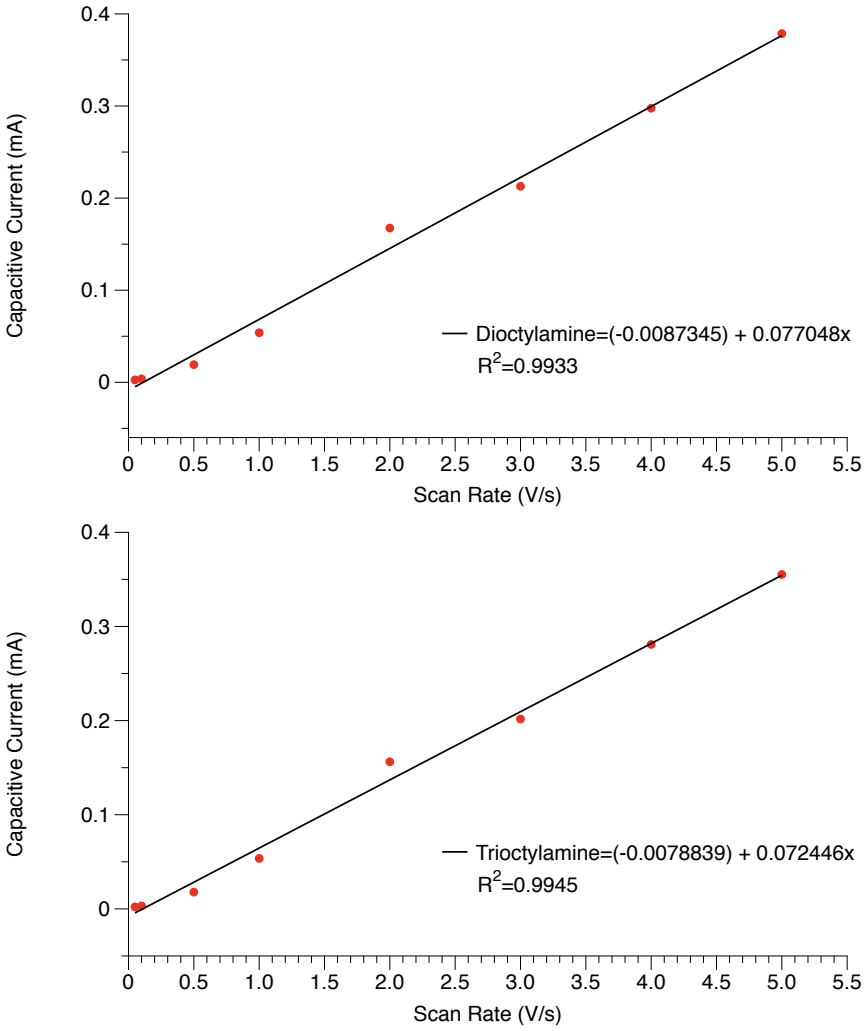


Figure 2.18. Capacitive current versus scan rate traces to measure $C_{DL}$ of the stripped, acetate, octanoate, butylamine, octylamine, dioctylamine, and trioctylamine treated CoP, respectively.

### 2.7.5 *Characterization methods*

TEM images were collected on an FEI Tecnai G2 F2O microscope. Powder XRD data was collected on a Bruker Microfocus instrument. Powder XRD samples were prepared by drop casting a solution of the as-synthesized CoP onto silicon <001> single crystal wafers. SEM images and EDS maps were collected on an FEI Sirion XL30 scanning electron microscope with an integrated energy dispersive x-ray spectrometer (EDS) from Oxford. FTIR spectra were

obtained on a Thermoscientific Nicolet-8700 spectrometer. Contact angle measurements were performed on a Kruss DSA100L drop shape analyzer on 3-mercaptopropyltrimethoxysilane treated glass slides. TGA was collected on Mettler Toledo TGA/DSC 3+ instrument.

### 2.7.6 *Preparation of 3-mercaptopropyltrimethoxysilane treated glass slides*

Glass slides were sonicated in solutions of soap, distilled water, acetone, and then isopropyl alcohol in order to clean substrates. After cleaning, the slides were submerged in a 5% v/v MPTS in toluene solution overnight. After treatment, the slides were washed with toluene three times, followed by sonication in a solution of toluene for 5 min. The glass slides were then rinsed and sonicated in an ethanol solution. The slides were dried in an oven at 160 ºC before use.[40] Multi-layer thick films were drop casted to ensure that the contact angle measurements were representative of the film rather than the glass support.

## 2.8 References


(1) Ung, D.; Cossairt, B. M. Effect of Surface Ligands on CoP for the Hydrogen Evolution Reaction. *ACS Appl. Energy Mater.* **2019**, *2* (3), 1642–1645.

(2) Boles, M. A.; Ling, D.; Hyeon, T.; Talapin, D. V. The Surface Science of Nanocrystals. *Nat. Mater.* **2016**, *15* (2), 141–153.

(3) Thanh, N. T. K.; Maclean, N.; Mahiddine, S. Mechanisms of Nucleation and Growth of Nanoparticles in Solution. *Chem. Rev.* **2014**, *114* (15), 7610–7630.

(4) Owen, J. S.; Park, J.; Trudeau, P.-E. E.; Alivisatos, a. P. Reaction Chemistry and Ligand Exchange at Cadmium-Selenide Nanocrystal Surfaces. *J. Am. Chem. Soc.* **2008**, *130* (37), 12279–12281.

(5) Owen, J. The Coordination Chemistry of Nanocrystal Surfaces. *Science (80-. ).* **2015**, *347* (6222), 615–616.

(6) McCrory, C. C. L.; Jung, S.; Ferrer, I. M.; Chatman, S.; Peters, J. C.; Jaramillo, T. F. Benchmarking Hydrogen Evolving Reaction and Oxygen Evolving Reaction Electrocatalysts for Solar Water Splitting Devices. *J. Am. Chem. Soc.* **2015**, No. 137, 4347–4357.

(7) Wills, A. W.; Kang, M. S.; Khare, A.; Gladfelter, W. L.; Norris, D. J. Thermally Degradable Ligands for Nanocrystals. *ACS Nano* **2010**, *4* (8), 4523–4530.

(8) Reisner, E.; Reisner, E. Ligand Removal from CdS Quantum Dots for Enhanced Photocatalytic H2 Generation in PH Neutral Water. *J. Mater. Chem. A Mater. energy Sustain.* **2016**, *4* (8), 2856–2862.

(9) Nelson, A.; Zong, Y.; Fritz, K. E.; Suntivich, J.; Robinson, R. D. Assessment of Soft Ligand Removal Strategies: Alkylation as a Promising Alternative to High-Temperature Treatments for Colloidal Nanoparticle Surfaces. *ACS Mater. Lett.* **2019**, 177–184.
(10) Li, D.; Wang, C.; Tripkovic, D.; Sun, S.; Markovic, N. M.; Stamenkovic, V. R. Surfactant Removal for Colloidal Nanoparticles from Solution Synthesis: The Effect on Catalytic Performance. *ACS Catal.* **2012**, *2* (7), 1358–1362.
(11) Drndić, M.; Jarosz, M. V.; Morgan, N. Y.; Kastner, M. A.; Bawendi, M. G. Transport Properties of Annealed CdSe Colloidal Nanocrystal Solids. *J. Appl. Phys.* **2002**, *92* (12), 7498–7503.
(12) Baik, S. J.; Kim, K.; Lim, K. S.; Jung, S.; Park, Y. C.; Han, D. G.; Lim, S.; Yoo, S.; Jeong, S. Low-Temperature Annealing for Highly Conductive Lead Chalcogenide Quantum Dot Solids. *J. Phys. Chem. C* **2011**, *115* (3), 607–612.
(13) Liu, M. Ligand Effects in Catalysis by Atomically Precise Gold Nanoclusters. *Wuli Huaxue Xuebao/ Acta Phys. - Chim. Sin.* **2018**, *34* (6), 553–554.
(14) Chu, S. B.; Fukushima, T.; Surendranath, Y. Minor Impact of Ligand Shell Steric Profile on Colloidal Nanocarbon Catalysis. *Chem. Mater.* **2017**, *29* (2), 495–498.
(15) Xu, G. R.; Bai, J.; Yao, L.; Xue, Q.; Jiang, J. X.; Zeng, J. H.; Chen, Y.; Lee, J. M. Polyallylamine-Functionalized Platinum Tripods: Enhancement of Hydrogen Evolution Reaction by Proton Carriers. *ACS Catal.* **2017**, *7* (1), 452–458.
(16) Benson, E. E.; Zhang, H.; Schuman, S. A.; Nanayakkara, S. U.; Bronstein, N. D.; Ferrere, S.; Blackburn, J. L.; Miller, E. M. Balancing the Hydrogen Evolution Reaction, Surface Energetics, and Stability of Metallic MoS 2 Nanosheets via Covalent Functionalization. *J. Am. Chem. Soc.* **2018**, *140* (1), 441–450.
(17) Morales-Guio, C. G.; Hu, X. Amorphous Molybdenum Sulfides as Hydrogen Evolution Catalysts. *Acc. Chem. Res.* **2014**, *47*, 2671–2681.
(18) Morales-Guio, C. G.; Stern, L.-A.; Hu, X. Nanostructured Hydrotreating Catalysts for Electrochemical Hydrogen Evolution. *Chem. Soc. Rev.* **2014**, *43* (18), 6555–6569.
(19) Habas, S. E.; Baddour, F. G.; Ruddy, D. A.; Nash, C. P.; Wang, J.; Pan, M.; Hensley, J. E.; Schaidle, J. A. A Facile Molecular Precursor Route to Metal Phosphide Nanoparticles and Their Evaluation as Hydrodeoxygenation Catalysts. *Chem. Mater.* **2015**, *27* (22), 7580–7592.
(20) Callejas, J. F.; Read, C. G.; Roske, C. W.; Lewis, N. S.; Schaak, R. E. Synthesis, Characterization, and Properties of Metal Phosphide Catalysts for the Hydrogen-Evolution Reaction. *Chem. Mater.* **2016**, *28* (17), 6017–6044.
(21) Shi, Y.; Zhang, B. Recent Advances in Transition Metal Phosphide Nanomaterials: Synthesis and Applications in Hydrogen Evolution Reaction. *Chem. Soc. Rev.* **2016**.
(22) Callejas, J. F.; Read, C. G.; Popczun, E. J.; McEnaney, J. M.; Schaak, R. E. Nanostructured Co2P Electrocatalyst for the Hydrogen Evolution Reaction and Direct Comparison with Morphologically Equivalent CoP. *Chem. Mater.* **2015**, *27* (10), 3769–3774.
(23) Saadi, F. H.; Carim, A. I.; Verlage, E.; Hemminger, J. C.; Lewis, N. S.; Soriaga, M. P. CoP as an Acid-Stable Active Electrocatalyst for the Hydrogen-Evolution Reaction: Electrochemical Synthesis, Interfacial Characterization and Performance Evaluation. *J. Phys. Chem. C* **2014**, *118* (50), 29294–29300.
(24) Popczun, E. J.; Read, C. G.; Roske, C. W.; Lewis, N. S.; Schaak, R. E. Highly Active Electrocatalysis of the Hydrogen Evolution Reaction by Cobalt Phosphide Nanoparticles.

*Angew. Chemie Int. Ed.* **2014**, *53* (21), 5427–5430.
(25) Sun, M.; Liu, H.; Qu, J.; Li, J. Earth-Rich Transition Metal Phosphide for Energy Conversion and Storage. *Adv. Energy Mater.* **2016**, *6* (13), 1–34.
(26) Yuan, H.; Chen, X.; Zhou, G.; Zhang, W.; Luo, J.; Huang, H.; Gan, Y.; Liang, C.; Xia, Y.; Zhang, J.; et al. Efficient Activation of Li2S by Transition Metal Phosphides Nanoparticles for Highly Stable Lithium-Sulfur Batteries. *ACS Energy Lett.* **2017**, *2* (7), 1711–1719.
(27) Enright, M. J.; Cossairt, B. M. Synthesis of Tailor-Made Colloidal Semiconductor Heterostructures. *Chem. Commun.* **2018**, *54* (52), 7109–7122.
(28) Puntes, V. F.; Krishnan, K. M.; Alivisatos, A. P. Colloidal Nanocrystal Shape and Size Control: The Case of Cobalt. *Science* **2001**, *291* (5511), 2115–2117.
(29) Iablokov, V.; Beaumont, S. K.; Alayoglu, S.; Pushkarev, V. V; Specht, C.; Gao, J.; Alivisatos, A. P.; Kruse, N.; Somorjai, G. A. Size-Controlled Model Co Nanoparticle Catalysts for CO2 Hydrogenation: Synthesis, Characterization, and Catalytic Reactions. *Nano Lett.* **2012**, *12*, 3091–3096.
(30) Rosen, E. L.; Buonsanti, R.; Llordes, A.; Sawvel, A. M.; Milliron, D. J.; Helms, B. A. Exceptionally Mild Reactive Stripping of Native Ligands from Nanocrystal Surfaces by Using Meerwein's Salt. *Angew. Chemie Int. Ed.* **2012**, *51* (3), 684–689.
(31) Henckel, D. A.; Lenz, O.; Cossairt, B. M. Effect of Ligand Coverage on Hydrogen Evolution Catalyzed by Colloidal WSe2. *ACS Catal.* **2017**, *7* (4), 2815–2820.
(32) Henckel, D. A.; Lenz, O. M.; Krishnan, K. M.; Cossairt, B. M. Improved HER Catalysis through Facile, Aqueous Electrochemical Activation of Nanoscale WSe2. *Nano Lett.* **2018**, *18* (4), 2329–2335.
(33) Bai, L.; Gao, L.; Conway, B. E. Problem of in Situ Real-Area Determination in Evaluation of Performance of Rough or Porous, Gas-Evolving Electrocatalysts Part 2.-Unfolding of the Electrochemically Accessible Surface of Rough or Porous Electrodes : A Case-Study with an Electrodeposited P. *J. Chem. Soc. Faraday Trans.* **1993**, *89* (2), 243–249.
(34) Seligson, A. L.; Trogler, W. C. Cone Angles for Amine Ligands. X-Ray Crystal Structures and Equilibrium Measurements for Ammonia, Ethylamine, Diethylamine, and Triethylamine Complexes with the (Bis(Dimethylphosphino)Ethane)Methylpalladium(II) Cation. *J. Am. Chem. Soc.* **1991**, *113* (7), 2520–2527.
(35) Froehlich, J. D.; Kubiak, C. P. The Homogeneous Reduction of CO2 by [Ni(Cyclam)]+: Increased Catalytic Rates with the Addition of a CO Scavenger. *J. Am. Chem. Soc.* **2015**, *137* (10), 3565–3573.
(36) Pool, D. H.; Stewart, M. P.; O'Hagan, M.; Shaw, W. J.; Roberts, J. A. S.; Bullock, R. M.; DuBois, D. L. Acidic Ionic Liquid/Water Solution as Both Medium and Proton Source for Electrocatalytic H2 Evolution by [Ni(P2N2) 2]2+ Complexes. *Proc. Natl. Acad. Sci. U. S. A.* **2012**, *109* (39), 15634–15639.
(37) Rigsby, M. L.; Wasylenko, D. J.; Pegis, M. L.; Mayer, J. M. Medium Effects Are as Important as Catalyst Design for Selectivity in Electrocatalytic Oxygen Reduction by Iron-Porphyrin Complexes. *J. Am. Chem. Soc.* **2015**, *137* (13), 4296–4299.
(38) DuBois, D. L. Development of Molecular Electrocatalysts for Energy Storage. *Inorg. Chem.* **2014**, *53* (8), 3935–3960.
(39) McCrory, C. C. L.; Jung, S.; Peters, J. C.; Jaramillo, T. F. Benchmarking Heterogeneous Electrocatalysts for the Oxygen Evolution Reaction. *J. Am. Chem. Soc.* **2013**, *135* (45), 16977–16987.

(40) Pallavicini, P.; Dacarro, G.; Galli, M.; Patrini, M. Spectroscopic Evaluation of Surface Functionalization Efficiency in the Preparation of Mercaptopropyltrimethoxysilane Self-Assembled Monolayers on Glass. *J. Colloid Interface Sci.* **2009**, *332* (2), 432–438.

# Chapter 3. Studying Transition Metal Phosphides in Non-Aqueous Electrolyte Conditions

## 3.1 Introduction

Heterogeneous electrocatalysts for the HER are generally studied in aqueous electrolyte conditions. This is because HER is typically studied as one of the half reactions for water splitting, the other half reaction being the oxygen evolution reaction (OER, water oxidation). While working in aqueous conditions has a lot of practical benefits, there are many complications in studying electrocatalysts in aqueous conditions due to water's "non-innocent" behavior as a solvent. For example, there is poor control over the identity of proton donors in aqueous conditions because water will interact with Brønsted acids to form $H_3O^+$, which becomes the effective proton donor regardless of what acid is used in aqueous conditions. Furthermore, since water has many intermolecular interactions due to its extensive hydrogen bonding, the reorganization of water solvent molecules can generate significant energetic barriers for electrocatalytic transformations. Transitioning studies into non-aqueous solvents allows us to choose specific proton donors with different steric profiles and strengths. It also enables the study of HER catalysts in intrinsically low $H^+$ concentration conditions, where the presence of proton relays will likely have a larger impact on the local proton concentration and therefore catalytic activity. Lastly, studying how the interface of electrocatalysts impacts activity in aqueous versus non-aqueous systems may lead to the development of new design principles for improved electrocatalysts.

Furthermore, the surfaces of nanoparticles can be quite dynamic in aqueous conditions. For example, a common aqueous electrolyte solution for HER studies is 0.5 M $H_2SO_4$. However,

colloidally synthesized nanocrystals are often capped with long chain carboxylate and amine surface ligands, such as oleate and oleylamine. The pKa of oleate and oleylammonium are ~10 in water, while the pKa of $H_2SO_4$ is -3.[1] If a nanocrystal with these surface ligands is exposed to a solution of 0.5 M $H_2SO_4$ for an extended duration, the surface will equilibrate to form the conjugate acids of the surface ligands, leaving a bare surface that is charge balanced by a counter anion. This dynamic surface will change the activity for HER, as seen in the LSVs in Figure 3.1. This creates a common practice to repeatedly cycle the working electrode under the catalytic conditions in order to equilibrate the catalyst surface when benchmarking heterogeneous electrocatalysts for HER, which can be time consuming and inefficient.[2–5] Operating in conditions where the activity evolves over time can also make it challenging to compare activities of modified catalysts, such as ones with proton relays attached.

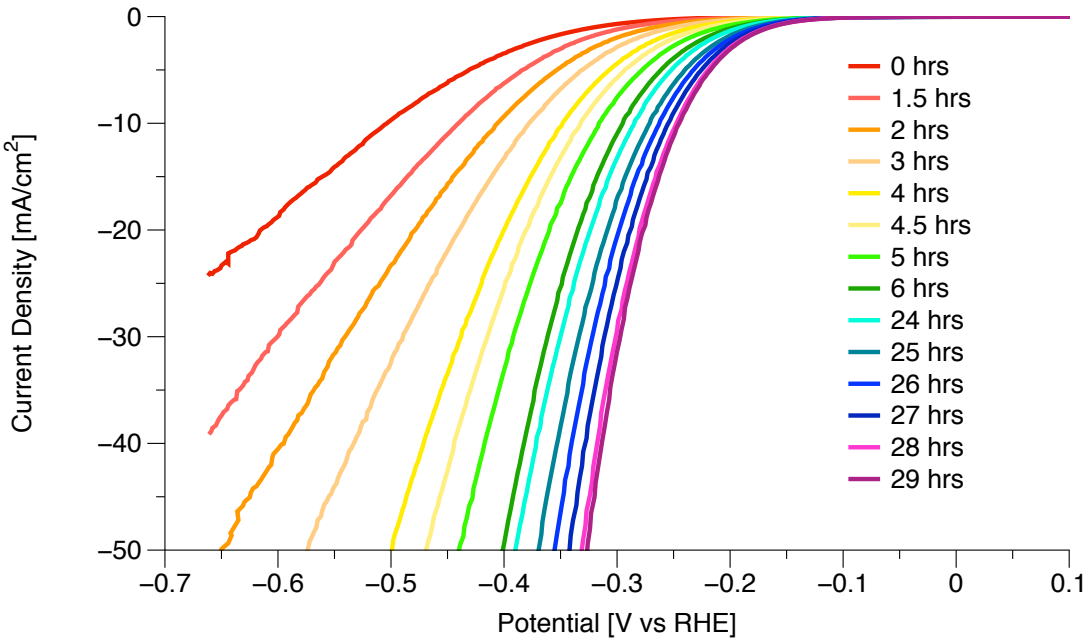


Figure 3.1. CoP functionalized with nonanoate, oleate, and oleylamine soaking in a solution of 0.5 M $H_2SO_4$ over a span of 29 hrs. The overpotential improves as the surface ligands equilibrate to form their conjugate acids.

## 3.2 The Role of pKa on Overpotential in Non-Aqueous Electrolyte

Adjusting the strength of the proton donor in aqueous conditions alters the extent to which the acid dissociates to form $H_3O^+$ ions, which then becomes the effective proton donor in solution that interacts with the catalyst. However, when operating in nonpolar aprotic solvents, the Brønsted acid used has a direct interaction with the catalyst, allowing for a range of acids with different pKa values and steric profiles to be tested.

It is important to note that buffering the organic acid is instrumental when studying organic acids in non-aqueous solutions, especially when using acids that can participate in homoconjugation such as dimethylformamidium.[6–9] This is because the solution composition at the electrode can vary significantly from that of the bulk solution. In the case of non-aqueous HER, a solution can be prepared with only the weak acid (HA) present, but once the catalyst begins to operate, the conjugate base ($A^-$) is generated (Figure 3.2). This changes the solution from an "infinitely unbuffered" state to a buffered state once catalytic current is passed in the system. This can lead to large errors in the measured overpotential due to homoconjugation of the weak acid, where the conjugate base can interact with the weak acid and alter its acidity. Preparing a buffered solution limits the differences between the bulk solution and the solution near the electrode and allows for consistent acid strength.[6,7]

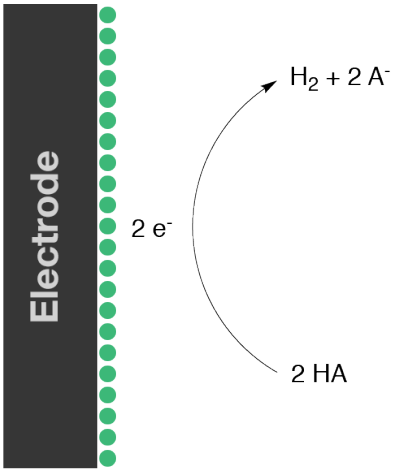


Figure 3.2. Diagram illustrating the transition from an infinitely unbuffered solution to a buffered solution once the electrocatalyst begins to operate and produces $H_2$ and generates $A^-$. This can lead to homoconjugation depending on the organic acid used.

For the electrochemical studies in this chapter, a typical three-electrode setup was used with $Ni_2P$ drop casted onto a carbon fiber working electrode, platinum counter electrode, and Ag pseudo reference electrode in a 0.1 M tetrabutylammonium hexafluorophosphate ($TBAPF_6$) electrolyte solution unless otherwise noted. Using this setup, a range of three different organic acids with different pKa values were tested: triethylammonium hexafluorophosphate ($[HNEt_3][PF_6]$), anilinium tetrafluoroborate (anilinium $[BF_4]$), and dimethylformamidium triflate ([H-DMF][OTf]).[9,10] The data collected shows that as the acidity of the proton donor increases (pKa decreases), the overpotential needed for HER decreases (Figure 3.3). This makes intuitive sense because as the proton becomes more easily donated, the energy barrier needed to form the adsorbed hydrogen intermediate decreases, and therefore the overpotential decreases (i.e. the energy needed to reach the transition state decreases with a more energetically accessible proton donor). Furthermore, these results show that there is a Nernstian dependence on the potential as a function of pKa (Figure 3.4). The potentials used to determine the Nernstian dependence were

taken at a current density of 1 mA/cm$^2$ to avoid any influences of mass transport on the potential for HER at higher current densities.

Table 3.3. pKa of organic acids used in the study

| Ligand | pKa in MeCN | Potential at 1 mA (V vs $Fc^{+/0}$) | Potential at 10 mA (V vs $Fc^{+/0}$) |
|---|---|---|---|
| $[HNEt_3][PF_6]$ | 18.82 | -1.26 | -1.57 |
| Anilinium $[BF_4]$ | 10.62 | -0.77 | -1.12 |
| [HDMF][OTf] | 6.1 | -0.53 | -1.01 |

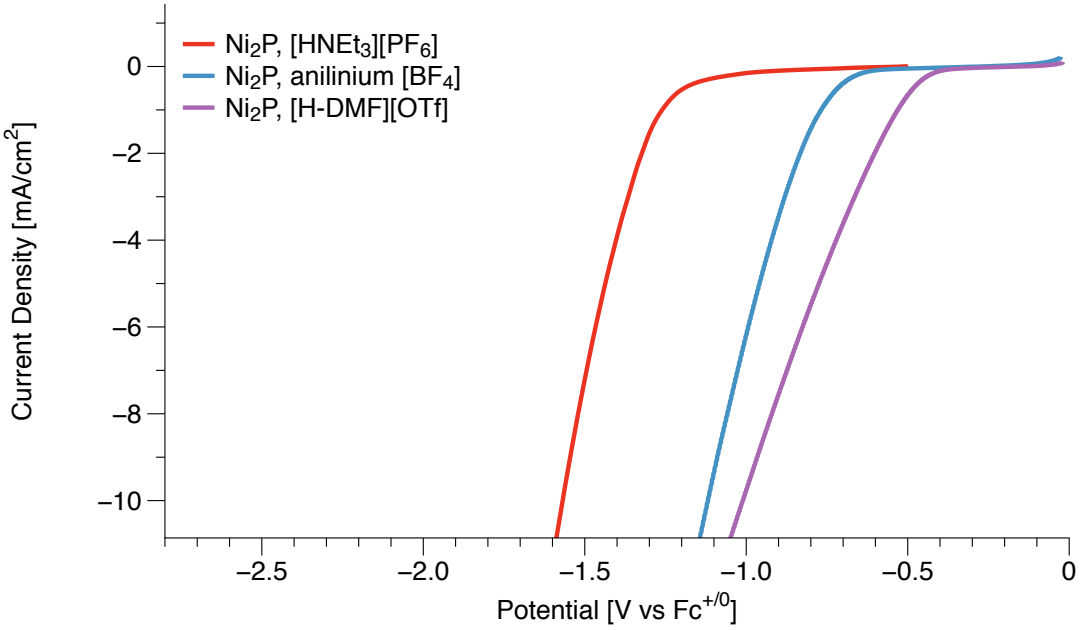


Figure 3.3. LSVs of $Ni_2P$ working electrodes with a range of proton donors.

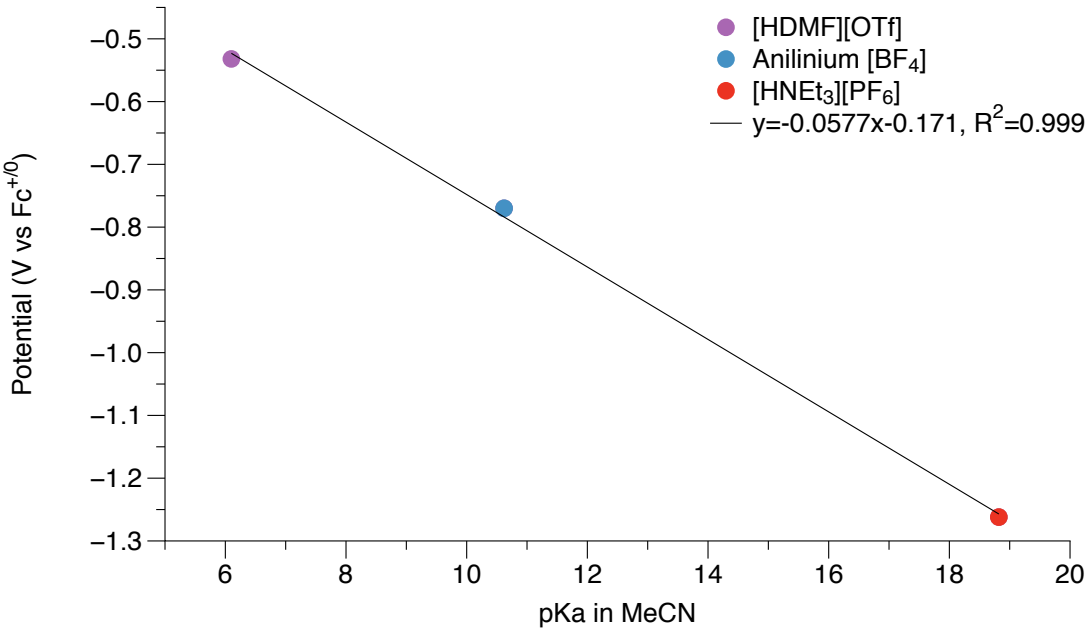


Figure 3.4. Potential at a current density of 1 mA/cm$^2$ versus pKa of the organic acids shows a Nernstian dependence.

Adjusting the pKa of the proton donor alters the thermodynamic starting point for the reaction by changing the reduction potential of the reactants. When this change in pKa is accounted for by correcting the potential by 59 mV per pKa unit, it is clear that the potential necessary to generate $H_2$ from the different proton donors are roughly the same (Figure 3.5). There are some differences in the overpotential necessary for HER at higher current densities which is likely caused by mass transport effects due to the varied diffusion coefficients of the different organic acids. This result illustrates that altering the pKa of the organic acid is a thermodynamic modification to the energy landscape, and that the kinetic barriers and transition states of the reaction are similar regardless of the organic proton donor used in non-aqueous electrolyte systems.

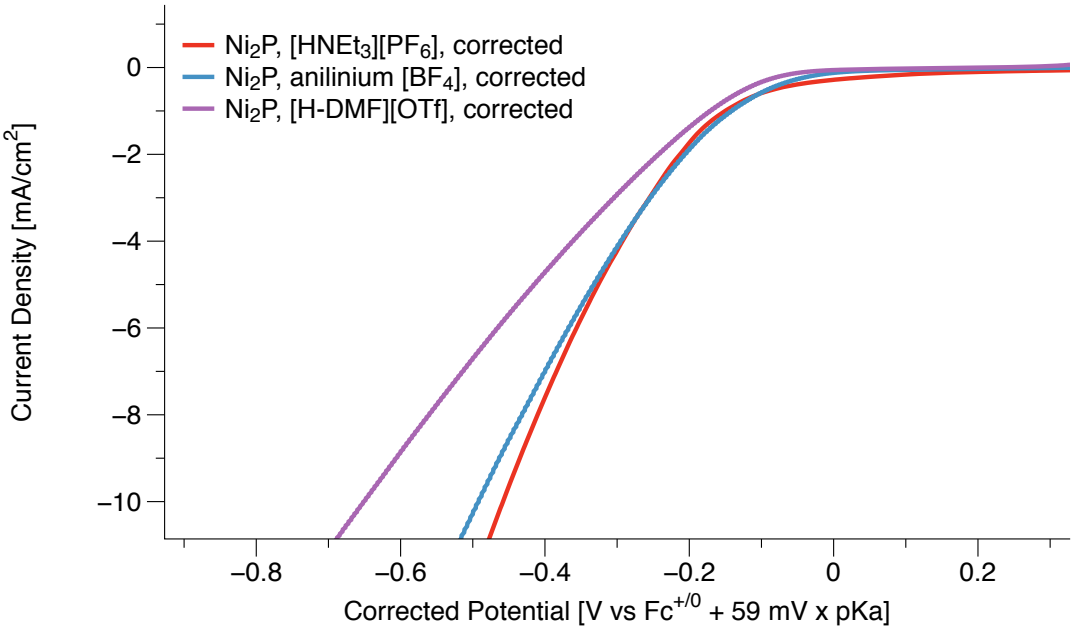


Figure 3.5. Correcting the potential of LSVs of $Ni_2P$ working electrodes with a range of proton donors by 59 mV per pKa unit shows similar electrocatalytic performance.

Changing the activity of the substrate in solution can also be done in aqueous systems by altering the pH of the solution. When referencing the potentials versus an absolute reference electrode such as the standard hydrogen electrode (SHE), there are large improvements in electrocatalytic activity when moving to acidic pH (Figure 3.6). However, it is common to take into account the activity of the substrate in aqueous systems by referencing versus the reversible hydrogen electrode (RHE), which has a pH correction term of 59 mV per pH unit (Figure 3.7). This correction is similar to the pKa correction term used for Figure 3.5. There are still large differences in electrocatalytic activity when comparing acidic and alkaline pH even after referencing versus RHE.

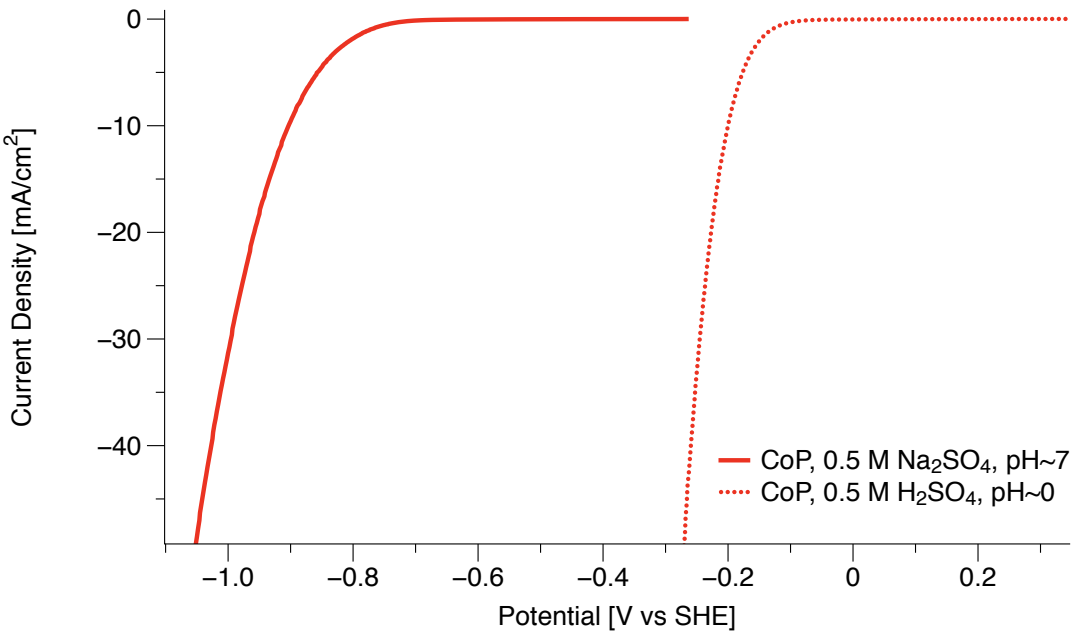


Figure 3.6. Overpotential for HER changes drastically as a function of pH in aqueous electrolyte conditions when referencing versus SHE.

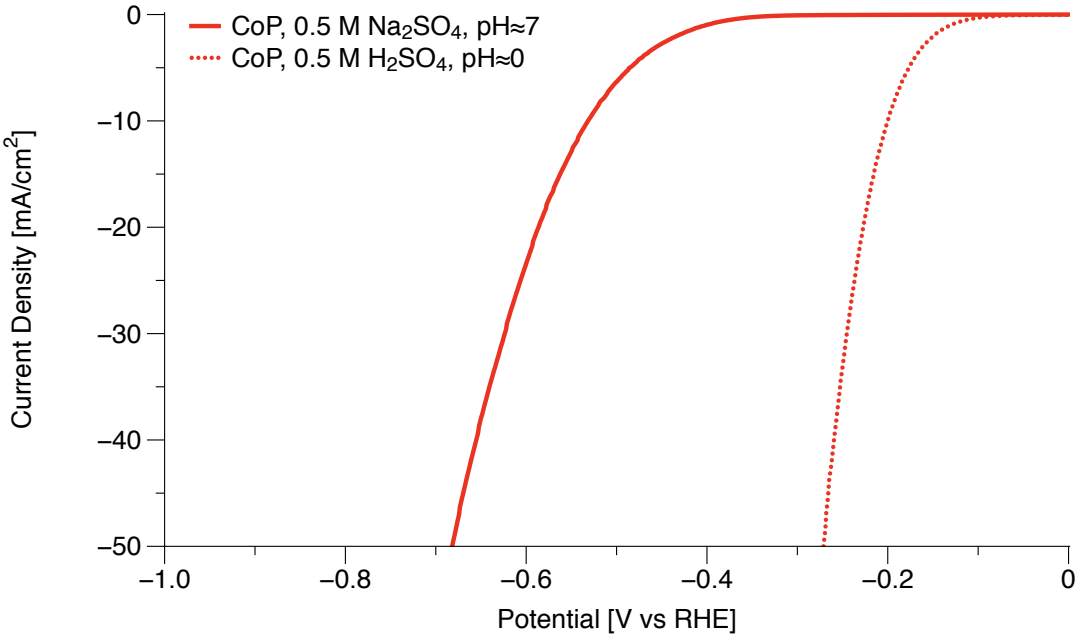


Figure 3.7. Introducing a pH correction term of 59 mV per pH unit still yields differences in overpotential in aqueous electrolyte conditions.

It is well known that proton concentration can have significant impacts in the overpotential in aqueous electrolyte. This pH dependence can be seen with a range of catalytic materials for HER, including transition metal phosphides and platinum catalysts.[11–14] However, the exact cause of the pH dependent overpotential is still an active area of research. One proposed explanation is that as the pH increases from acidic to neutral/alkaline pH, the identity of the proton donor changes from $H_3O^+$ ion to neutral $H_2O$.[14] This change in proton donor can adjust the starting potential of the reactants for HER and can alter the thermodynamic barrier for the reaction to proceed. This explanation is similar to adjusting the pKa in non-aqueous systems as described above. Another common explanation for the pH dependent overpotential is that the pH of the solution can alter the structure of interfacial solvent molecules and therefore impact the solvent reorganization energy associated with the catalytic transformation.[12] This explanation is supported by the LSVs seen in Figure 3.7, where correcting for the activity of the proton donor in aqueous systems still yields large differences in overpotential. This shows that the kinetic barriers and transition state energies can greatly differ at different pH in aqueous solvent. Altering the reorganization energy of a reaction necessarily changes the activation energy, as seen in Figure 3.8.

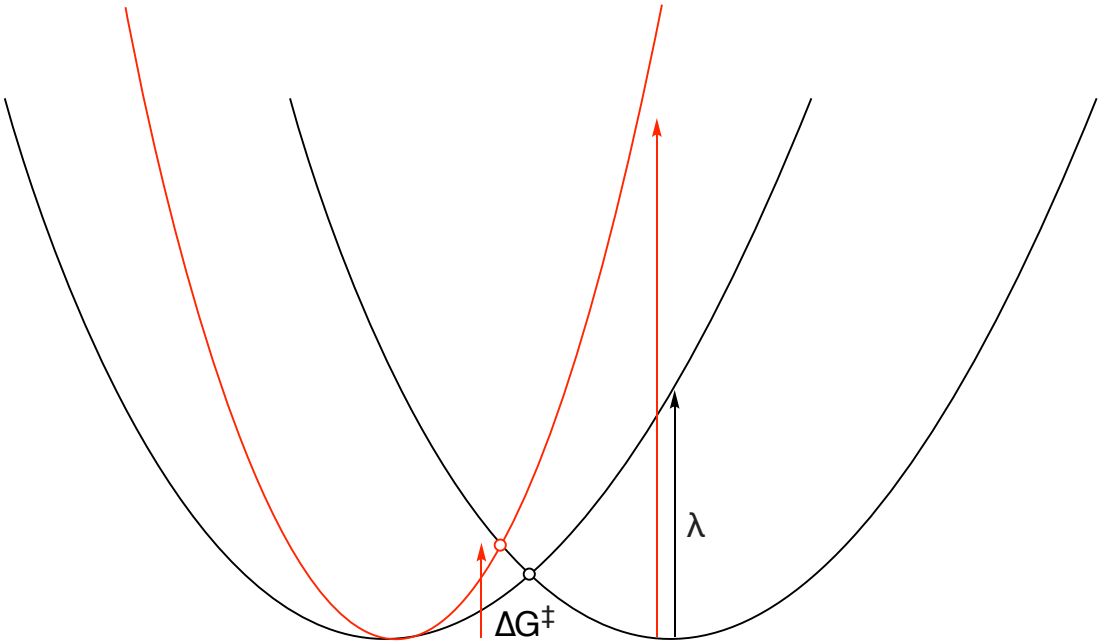


Figure 3.8. Increasing the reorganization energy (λ) by either translating the parabola or narrowing it requires an increase in the activation energy ($\Delta G^{\ddagger}$).

These results show that working in non-aqueous systems is an incredibly powerful tool to understand electrocatalysts for HER because it allows for studies where the thermodynamic descriptors of the reaction are adjusted without altering the kinetic barriers associated with the transformation. Working in aqueous solvent necessarily convolutes the system because it is impossible to decouple the thermodynamic descriptors (e.g. strength of the proton donor) from the kinetic barriers (e.g. transition state energies).

## 3.3 Aliphatic Surface Ligands Form a Favorable Interface With Non-Aqueous Electrolyte Solutions

A major conclusion of the work presented in chapter 2 of this dissertation is that one of the main factors by which traditional aliphatic surface ligands decrease catalytic activity for HER is by impeding substrate access to the catalytically active surface by creating an extremely hydrophobic interface between the material and the bulk electrolyte solution. By removing the surface ligands, there is both improved access to the surface by lowering the amount of steric bulk and also by improving the electrode-electrolyte solution interface. This can be seen by an increase in the capacitive current, which also corresponds to an increase in the ECSA.

Contrary to what is observed in water, no change in overpotential can be seen when stripping $Ni_2P$ working electrodes with Meerwein's reagent and testing the catalytic activity in non-aqueous electrolyte solutions with an organic proton donor (Figure 3.9). Regardless of the proton donor used, each LSV trace of the stripped samples overlay exactly on top of the as-synthesized scans.

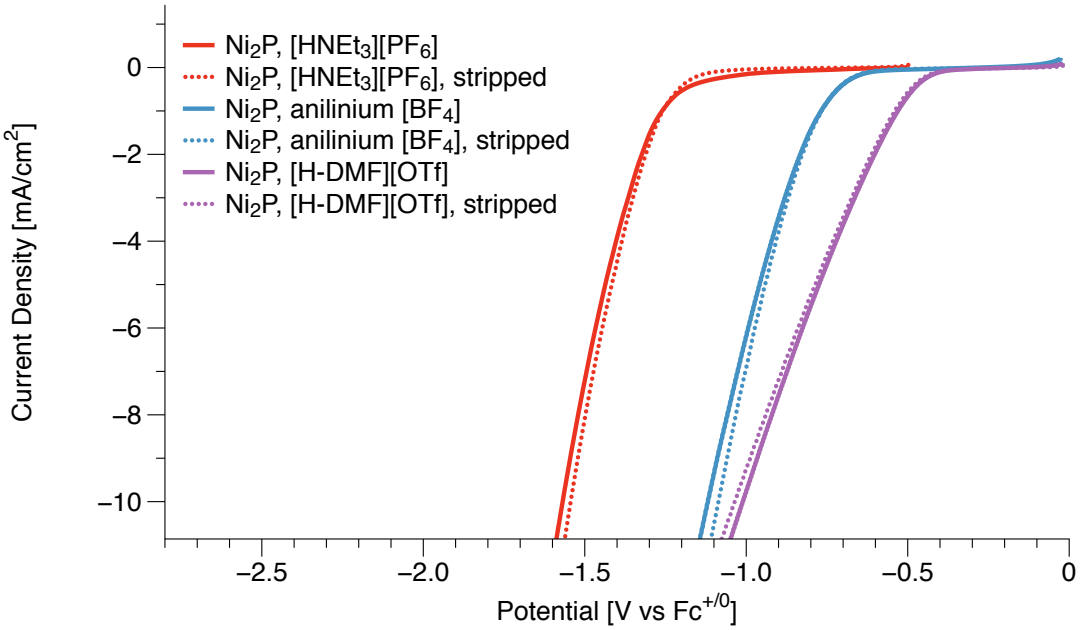


Figure 3.9. Stripped $Ni_2P$ electrodes overlaid with as-synthesized $Ni_2P$ show no change in overpotential.

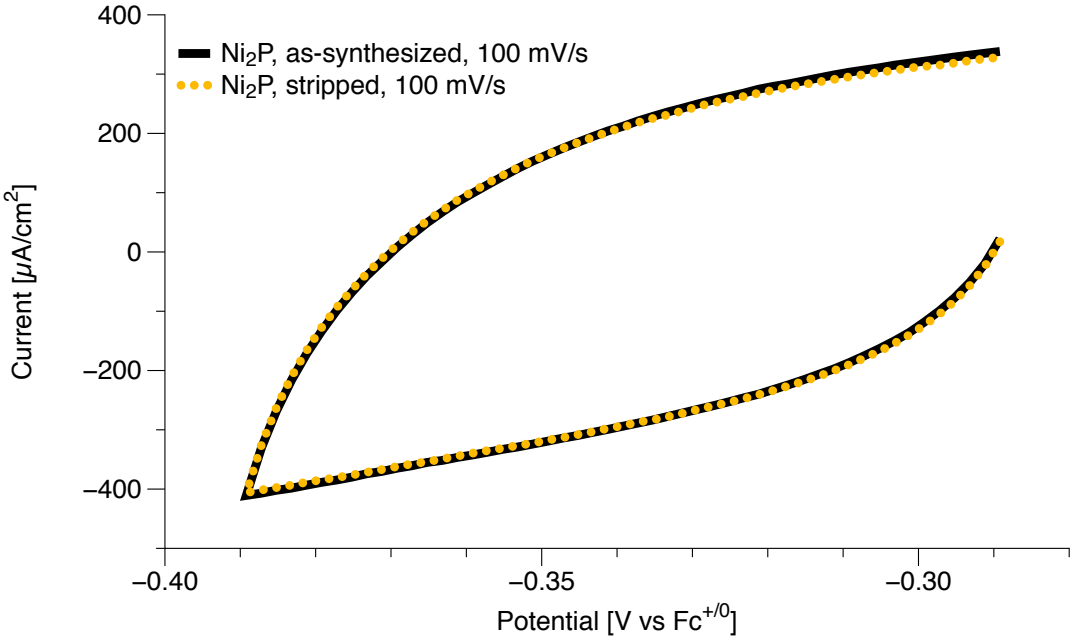


Figure 3.10. Capacitive current (and therefore ECSA) of $Ni_2P$ is unchanged after treatment with Meerwein's reagent in a non-aqueous electrolyte solution.

We propose that this is because the traditional aliphatic surface ligands used for transition metal phosphide syntheses (trioctylphosphine, oleylamine, oleate) all form favorable interfaces with non-aqueous solvents due to their relatively low polarity. This is clear when comparing the different contact angles of a droplet of water versus a droplet of acetonitrile (Figure 3.11). The water droplet has a high contact angle with an as-synthesized $Ni_2P$ film and decreases significantly when the film is treated with Meerwein's reagent. In contrast, the droplet of MeCN already has an extremely low contact angle with the as-synthesized film of $Ni_2P$ (< 40º), which has a small change when stripped with Meerwein's reagent. A 0.1 M $TBAPF_6$ MeCN solution was prepared for the contact angle measurements to better emulate the electrochemical conditions with a more polar electrolyte solution.

This is further evident when looking at the change in capacitive current before and after exposure to Meerwein's reagent. As-synthesized $Ni_2P$ and the stripped $Ni_2P$ have the same capacitive current, suggesting that the surface area of the electrode is not changed (Figure 3.10). This result shows further evidence that the aliphatic tails on the surface ligands of $Ni_2P$ form a favorable interface with electrolyte solution, where the solvent and electrolyte is still able to access the vast majority of the surface of the electrode. The surface ligands do not perturb the formation of a full double layer across the surface of the electrode at the interface (Figure 3.12).

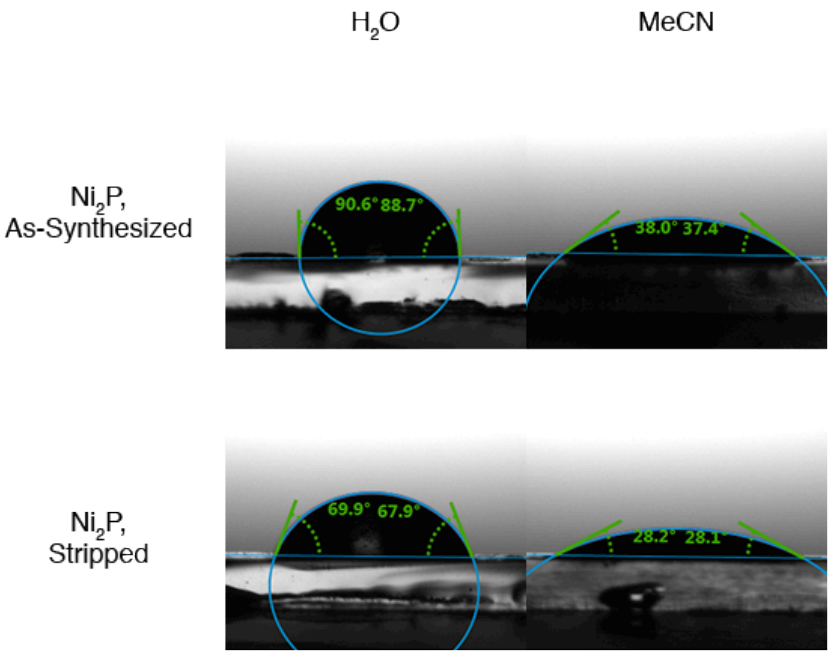


Figure 3.11. Contact angle measurements of as-synthesized and stripped $Ni_2P$ with water and MeCN.

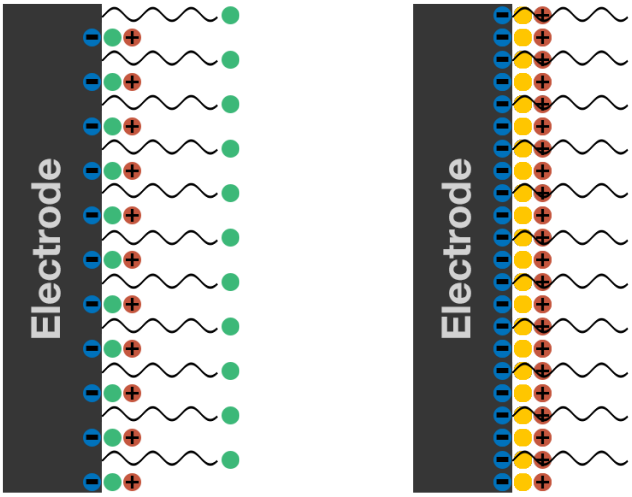


Figure 3.12. Diagram illustrating how the long chain tails of surface ligands prevent aqueous solvent (green circles) from reaching the electrode but organic solvent (orange circles) is able to form a full double layer.

## 3.4 How Does Proton Donor Concentration Impact Activity in Non-Aqueous Electrolyte Solutions?

The effect of proton donor concentration on electrocatalytic activity can be studied by titrating a stock solution of weak acid into the electrolyte solution. A 10:1 $HA:A^-$ stock solution of [H-DMF][OTf] at concentration of 1.6 M was prepared and titrated into a standard electrochemical cell in 100 μL increments (Figure 3.13). The first observation is that as the concentration of acid is increased, so does the catalytic current. At high current densities, the slope of the catalytic current starts to tail off as it reaches diffusion limited regimes. However, the onset potential for where the catalytic current starts to take off is constant, regardless of the concentration of the acid. This fixed onset potential is due to the titration of the buffered $HA:A^-$ solution. The ratio of the weak acid to the conjugate base stays constant, and therefore the onset potential doesn't shift as a function of acid concentration, as seen in equation 3.1.

$$E = E^0 - \frac{RT}{nF} ln \frac{[H_2][A^-]^2}{[HA]^2} \qquad \text{Equation 3.1}$$

Another important note is that there is no underpotential deposition, and there is no "minimum" concentration of proton donor needed for catalysis to turn on. The catalytic current observed is relatively broad, which is likely due to a combination of factors. First, a sample of colloidally synthesized nanocrystals often has a distribution of sizes. Each of these sizes will have slightly different reactivity due to the differences in surface chemistry. Furthermore, there are multiple facets on a given nanocrystal that can also have varying reactivity. Second, the transport of a proton donor through MeCN may be much more sluggish when compared to aqueous conditions. In aqueous conditions, the solvent acts as a proton shuttle and is able to

effectively transport the proton through a hydrogen bonding network. However, in non-aqueous systems the proton donor may need to displace solvent molecules as it diffuses to the electrode. Finally, there may be sluggish electron transfer kinetics due to the insulating nature of the long chain hydrocarbons on the surface of $Ni_2P$ on the electrode.

One concern of using [H-DMF][OTf] as a proton source in MeCN is that it is known to homoconjugate with its conjugate base in MeCN. As the concentration of the buffer solution increases, the amount of monomeric [H-DMF][OTf] may change. This equilibrium concentration can be calculated when factoring in the homoconjugation constant $K_f$=49 $M^{-1}$ for $[H\text{-}DMF]^+$ in MeCN.[15] Figure 3.14 shows that the amount of monomeric [H-DMF][OTf] is only slightly decreased at the buffer concentrations used in the studied catalytic conditions, and that the overall behavior of the catalyst is similar at a potential of -1 V vs $Fc^{+/0}$ which is well outside the diffusion-limited current regime.

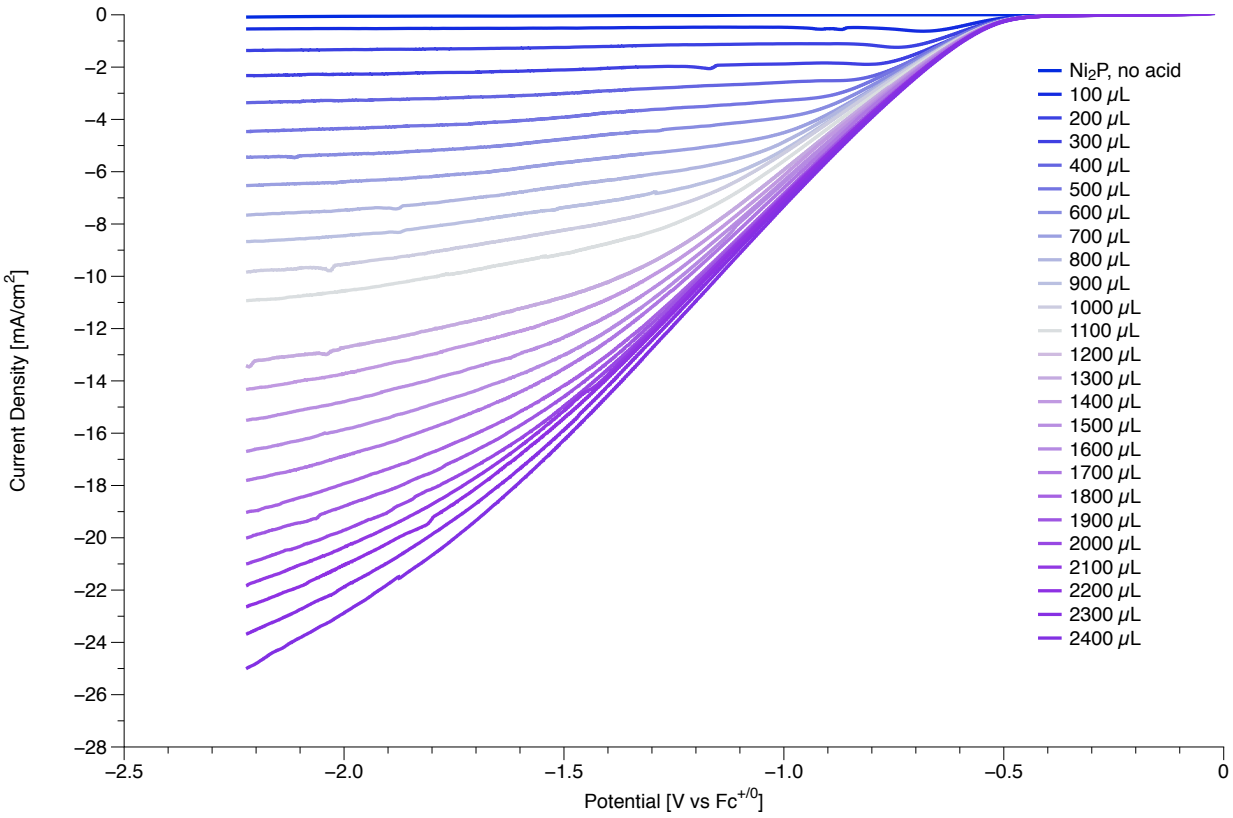


Figure 3.13. Increasing acid concentration doesn't alter the onset potential for HER with [H-DMF][OTf] as the proton donor.

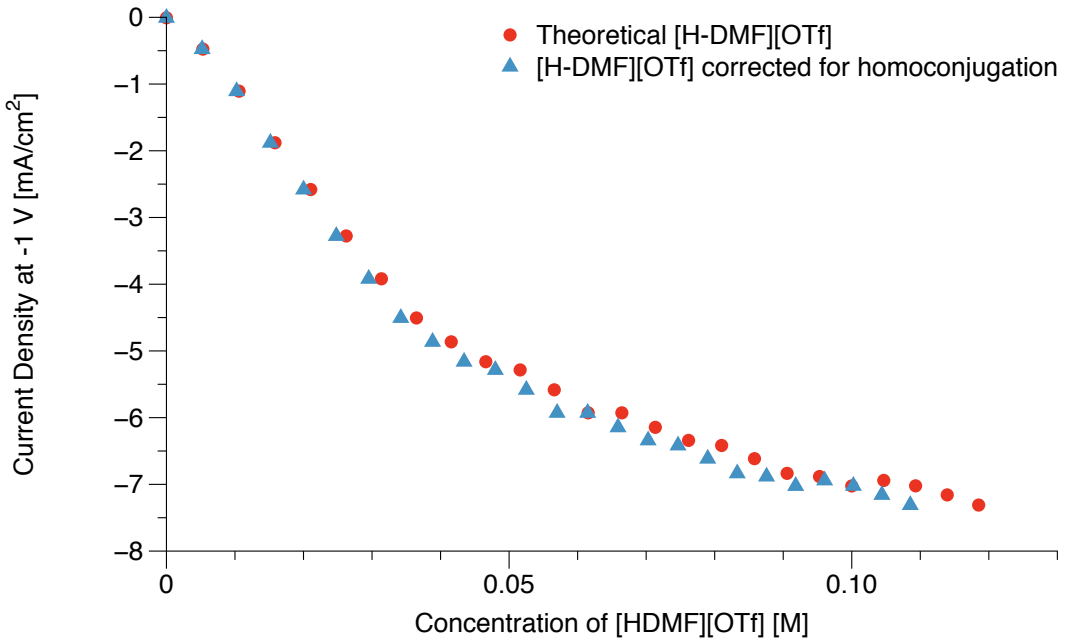


Figure 3.14. Correcting for $[H\text{-}DMF]^+$ homoconjugation shows similar electrocatalytic response.

## 3.5 Bifunctional Surface Ligands as Proton Relays

One major kinetic barrier for many catalytic transformations is the coupled movement of protons and electrons. In order for these transformations to occur, the proton and electron need to be at the right place at the right time. This is a common source of high overpotentials for synthetic catalysts.[16] However, many enzymes are highly engineered and are able to perform these complex multi-proton, multi-electron reactions at ambient pressures and temperatures. For example, [FeFe]hydrogenase enzymes are able to rapidly perform a two proton, two electron reduction to $H_2$ gas with nearly zero overpotential.[17,18] One key design feature in these highly efficient enzymes is the presence of a proton relay to aid in proton movement during catalysis (Figure 3.15). Proton relays have begun to be incorporated in many molecular catalysts in the secondary and outer coordination spheres.[17] The presence of these proton relays aid in inter- and intramolecular proton transfer, which facilitates the movement of protons in the reaction and greatly improves the overpotentials.

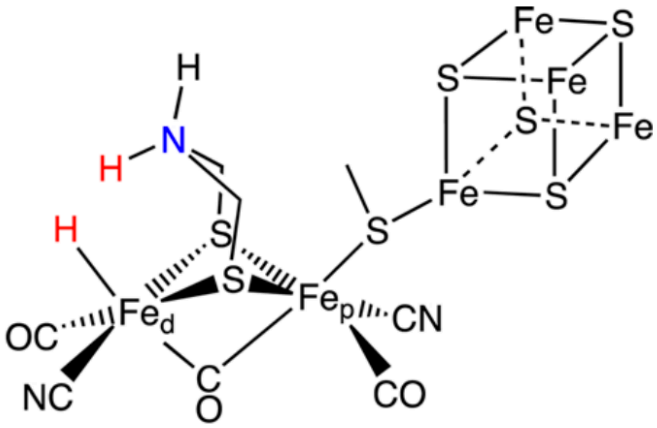


Figure 3.15. The structure of [FeFe]hydrogenase employs the use of a proton relay in the form of a pendant amine (blue) to aid in the movement of protons. Source: DuBois, D. L. Development of Molecular Electrocatalysts for Energy Storage. *Inorg. Chem.* **2014**, *53* (8), 3935–3960.

These organic ligands are considered an important synthetic tool to tune the behavior of molecular transition metal coordination complexes by modifying properties such as the electronic structure or steric profile of the molecule. Chemists can synthesize molecular catalysts with a variety of ligands to tune the reactivity, selectivity, and stability of the complex, using design principles developed over decades of scientific research.[19–23] In contrast, ligands are generally considered a detriment to the reactivity of nanomaterial catalysts due to inhibiting access to the catalytically active surface and are commonly removed via thermal or chemical treatments. However, there has been some recent progress in implementing cooperative surface ligands on nanomaterials that have been shown to improve catalytic activity.[24–27] For example, diamines surface ligands have been shown to improve HER activity in aqueous alkaline conditions when compared to single, primary amines. It is proposed that the presence of the terminal amine at the interface of the catalyst and the aqueous electrolyte solution improves the adsorption of water molecules and their transportation to the catalyst surface.[24] The presence of surface ligands that increase the effective local concentration of substrate which improves electrocatalytic activity can also be seen in the case of polyallylamine-capped Pt tripods, where the onset overpotential is more positive than the theoretical equilibrium potential of HER in aqueous acidic conditions because the local proton concentration is increased by orders of magnitude compared to the bulk solution.[25] These examples show the positive impact having a terminal functional group that can behave as a proton relay can have on catalytic activity on nanoparticles in aqueous conditions.

However, when stripped $Ni_2P$ working electrodes were treated with a solution of ethylenediamine, no change in the electrocatalytic activity was seen in non-aqueous electrolyte conditions with [H-DMF][OTf] as the proton donor (Figure 3.16). We hypothesized that this

may be caused by low density of the ethylenediamines on the surface of the $Ni_2P$ due to the weaker binding of neutral L-type amine ligands, as seen in chapter 2. However, similar results were seen when a stripped $Ni_2P$ working electrode was treated with the tetrabutylammonium salt of ß-alanine (Figure 3.16). The tetrabutylammonium salt was prepared for improved solubility in acetonitrile. These results suggest that the presence of terminal head groups that can participate as proton relays may not be an effective strategy for improving electrocatalytic performance of transition metal phosphides for HER in non-aqueous electrolyte conditions. It also suggests that the primary effect the ethylenediamine and polyallylamine surface ligands had on the HER electrocatalysts mentioned above were improvements in the electrode-electrolyte interface. The terminal amine groups are able to interact with the aqueous solvent, potentially participating in the hydrogen-bonding network. This improves the interaction with the proton donor ($H_2O$ or $H_3O^+$), but perhaps more importantly limits the solvent reorganization required at the electrode interface. Similar results have been seen in the literature on Ag nanoparticle catalysts for $CO_2RR$, where imidazolium surface ligands can be used to tune the selectivity for $CO_2RR$ in aqueous conditions. The changes in electronic structure with different surface ligands actually play a very small role in activity, and the majority of the improvements to reactivity are credited to the length of the hydrocarbon tail changing the interaction of the catalyst with the bulk solvent by altering the steric profile and hydrophobicity of the catalytically active surface.[27]

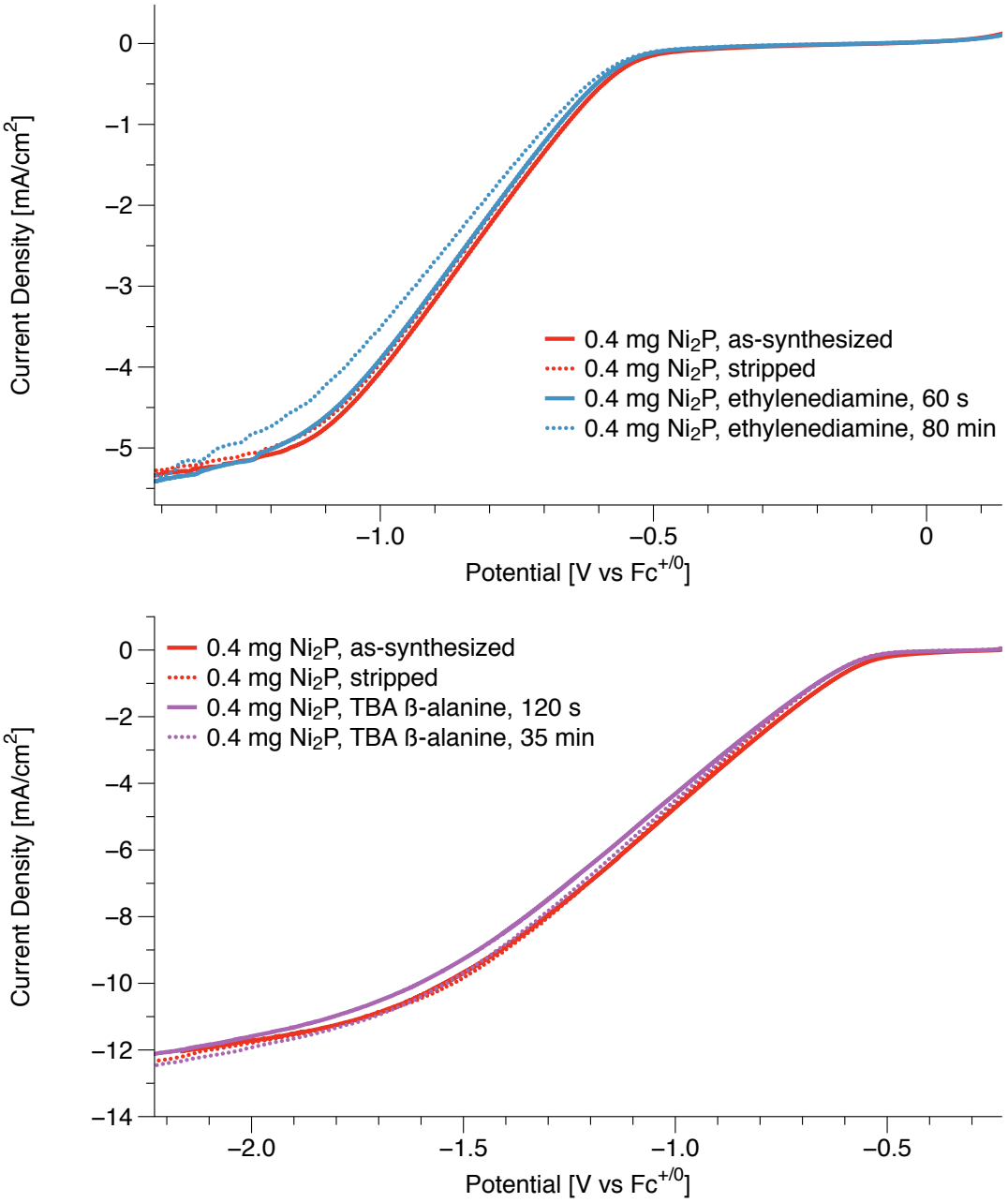


Figure 3.16. Treating a stripped $Ni_2P$ electrode with ethylenediamine (top) or tetrabutylammonium ß-alanine salt does not change its electrocatalytic activity.

This result combined with the conclusions gathered at the end of chapter 2 illustrates the critical role the electrode-electrolyte interface plays in electrocatalytic activity. In fact, it allows us to take a step back and realize that the typical thought process of improving overpotential of a

nanomaterial electrocatalyst by removing its surface ligands and increasing the number of active sites is actually perplexing. Increasing the number of active sites of a heterogeneous catalyst can be considered analogous to increasing the concentration of a homogeneous catalyst in solution. In this case, one would expect the rate of the reaction to increase because the increased concentration of catalyst, but a change in the energetic profile of the reaction is not expected, and therefore the onset overpotential of the catalyst should not change. However, if the surface ligands are altering the solvent and electrolyte's organization and packing at the interface, this can lead to changes in the energetic profile and therefore the overpotential of the reaction.

This critical role that ligands have on the interaction of a catalyst with the electrolyte solution has also been seen in other systems. For example, molecular $Ni(P_2N_2)_2$ catalysts have been studied in ionic liquids for HER.[17,18] The TOF for the different $P_2N_2$ ligands studied tracks with the hydrophobicity of the substituents on the ligand rather than the expected thermodynamic driving force for $H_2$ release from the intermediate. This result suggests that the outer-sphere ligand interactions with the ionic liquid solvent and electrolyte are critical to electrocatalytic activity. There has also been work done on iron porphyrin catalysts for the oxygen reduction reaction (ORR) that shows different reactivity depending on how the heterogeneous film is prepared.[28] This result shows that the organization of the surrounding medium, beyond the catalyst film, can have a substantial role in catalysis which can be seen as analogous to outer-sphere solvent effects on activity.

## 3.6 Conclusions

Studying $Ni_2P$ electrocatalysts in non-aqueous electrolyte conditions illustrates how complex aqueous electrolyte solutions are in comparison, due to the "non-innocent" behavior of $H_2O$ as a solvent. $H_2O$ has the ability to interact with itself and form hydrogen bonding networks,

as well as interacting with the substrate and becoming the proton donor in aqueous HER conditions. On the other hand, acetonitrile is a comparatively nonpolar aprotic solvent and has very few intermolecular interactions. Because of this, we are able to select proton donors with specific pKa values. As we increase the acidity of the proton donor (i.e. the proton is more readily available), the required overpotential for HER decreases due to the change in reduction potential of the reactants as a function of pKa. Correcting for this thermodynamic modification to the system yields very similar overpotentials necessary for HER, regardless of the organic acid used. This is extremely different when compared to aqueous systems, where correcting for the activity of the substrate by referencing versus RHE still yields large differences in overpotential. This illustrates that the solvent reorganization energy of the system can be greatly influenced by pH, and when the reorganization energy is increased, the activation energy has to be increased as well. Working in non-aqueous systems becomes an extremely powerful tool to understand the behavior of electrocatalysts because the thermodynamic descriptors of the system can be modified (e.g. pKa of the organic acid) without altering the kinetic barriers (e.g. transition state energies). Aqueous systems are more convoluted because it is impossible to decouple the thermodynamic and kinetic barriers in the system due to $H_2O$ having hydrogen bonding interactions as a solvent.

When changing the concentration of a buffered organic acid in non-aqueous solutions, we see that the only change is increased current at a given potential (e.g. faster rates), but the onset potential of the reaction does not change. The onset potential is stable because of the buffered solution keeping the ratio of weak acid and conjugate base fixed. However, the current tails off at high current densities due to reaching a diffusion limited current regime because MeCN is unable

to participate as a proton donor, unlike $H_2O$. The catalytic feature of the LSV is quite broad, which is likely due to the differences in activity as a function of particle size and facets.

Finally, when surface ligands equipped with terminal amines which can behave as proton relays are added to a $Ni_2P$ electrocatalyst in non-aqueous electrolyte, there is no change in the activity. These results in non-aqueous conditions illustrate how modifications to the surface ligation of a nanomaterial electrocatalyst can play large roles in the overpotential primarily by impacting the behavior of the electrode-electrolyte interface. When the interface is already favorable, adjusting the surface ligation may have very little effect. This shows a path moving forward on designing nanomaterials with favorable interfaces for specific applications in the future.

## 3.7 Outlook

It is well known that platinum is considered the state of the art material for electrocatalytic HER. This has widely been attributed to its thermoneutral $\Delta G_H$ of the required adsorbed-hydrogen intermediate to produce $H_2$.[29] However, not only does it have a thermoneutral intermediate, but pristine surfaces of platinum are known to be extremely hydrophilic.[30] The results presented in this dissertation show that the outer-coordination sphere ligand interactions with solvent can play a critical role in electrocatalytic activity. This suggests that the hydrophilic nature of Pt may be a key component in its high activity for HER, and that designing favorable interfaces in other electrocatalysts may be a method for improving electrocatalytic activity.

Furthermore, interfacial design can be utilized to tune the outer-coordination sphere environment without greatly impacting the electronic structure of the catalyst. This could be used to improve selectivity for more complicated multi-proton, multi-electron transformations such as

$CO_2RR$ or nitrogen reduction by controlling the effective local concentration of $H^+$ near the catalyst and reducing the amount of competitive HER.

## 3.8 Experimental

### 3.8.1 *Materials*

Nickel (II) acetylacetonate ($Ni(acac)_2$, Sigma-Aldrich), dioctyl ether (99%, Sigma-Aldrich), trioctylphosphine (TOP, Sigma-Aldrich, stored in glovebox), 2-propanol (anhydrous, 99.5%, Sigma-Aldrich, stored in glovebox), triethyloxonoium tetrafluoroborate (≥97.0%, Meerwein's reagent, Sigma-Aldrich, stored in glovebox), acetonitrile (anhydrous, 99.8% MeCN, Sigma-Aldrich, stored in glovebox), toluene (HPLC grade, Fisher), 3-mercaptopropyltrimethoxysilane (MPTS, Sigma-Aldrich), ß-alanine (99%, Sigma-Aldrich), tetrabutylammonium hydroxide (technical grade, ~40% solution in $H_2O$, Fluka Analytical), triethylammoinum chloride (Sigma-Aldrich), trifluoromethanesulfonic acid (triflic acid, ReagentPlus, >99%, Sigma-Aldrich, stored in glovebox), tetrafluoroboric acid diethyl ether complex (Sigma-Aldrich, stored in glovebox), and sodium hexafluorophosphate (ACS Reagent, >99.5%, Sigma-Aldrich) were used as received unless otherwise noted. Oleylamine (technical grade, 90%, Sigma-Aldrich) was dried over $CaH_2$, distilled, and stored over 4 Å molecular sieves in a nitrogen-filled glovebox. Ethylenediamine (99%, extra pure, Acros), N,N-dimethylformamide (DMF, Certified ACS, Fisher), and aniline (ReagentPlus, 99%, Sigma-Aldrich) were dried over 4 Å molecular sieves, distilled, and stored over 4 Å molecular sieves in a nitrogen-filled glovebox. Tetrabutylammonium hexafluorophosphate ($TBAPF_6$, >98%, TCI) was recrystallized in ethanol three times and dried under vacuum before use as an electrolyte for electrochemical measurements. Ferrocene (98%, Sigma-Aldrich) was recrystallized in hexanes twice and dried under vacuum before use as an internal reference.

### 3.8.2 *Synthesis of $Ni_2P$ nanoparticles*

All glassware was dried in a 160º C oven overnight prior to use. All reactions, unless otherwise noted, were run under an inert atmosphere of nitrogen using a glovebox or using standard Schlenk techniques. Synthesis was adapted from Brock *et al.*[17,18,28] $Ni(acac)_2$ (2.055 g, 8 mmol) and dioctyl ether (20 mL, 33.2 mmol) were added to a 100 mL 3-neck round bottom flask, equipped with a septum, thermowell, two stacked condensers, and a stir bar. The reaction flask was degassed under vacuum at 120 ºC for 1 hour. While degassing, oleylamine (8 mL, 24 mmol) and trioctylphosphine (TOP, 20 mL, 44.8 mmol) were injected via syringe. The reaction flask was heated to 230 ºC for 80 mins. The temperature was then raised to 270 ºC (reflux) and heated for 5.5 hrs. The reaction flask was then removed from heat, and 18 mL (56 mmol) of oleylamine was immediately injected to quench the reaction and to improve the colloidal stability of the nanoparticles. The resulting nickel phosphide nanoparticles were purified in a glovebox by washing with isopropyl alcohol, followed by centrifugation at 11000 rpm for 10 mins. The particles were then resuspended in toluene and washed with additional isopropyl alcohol and centrifuged an additional two times.

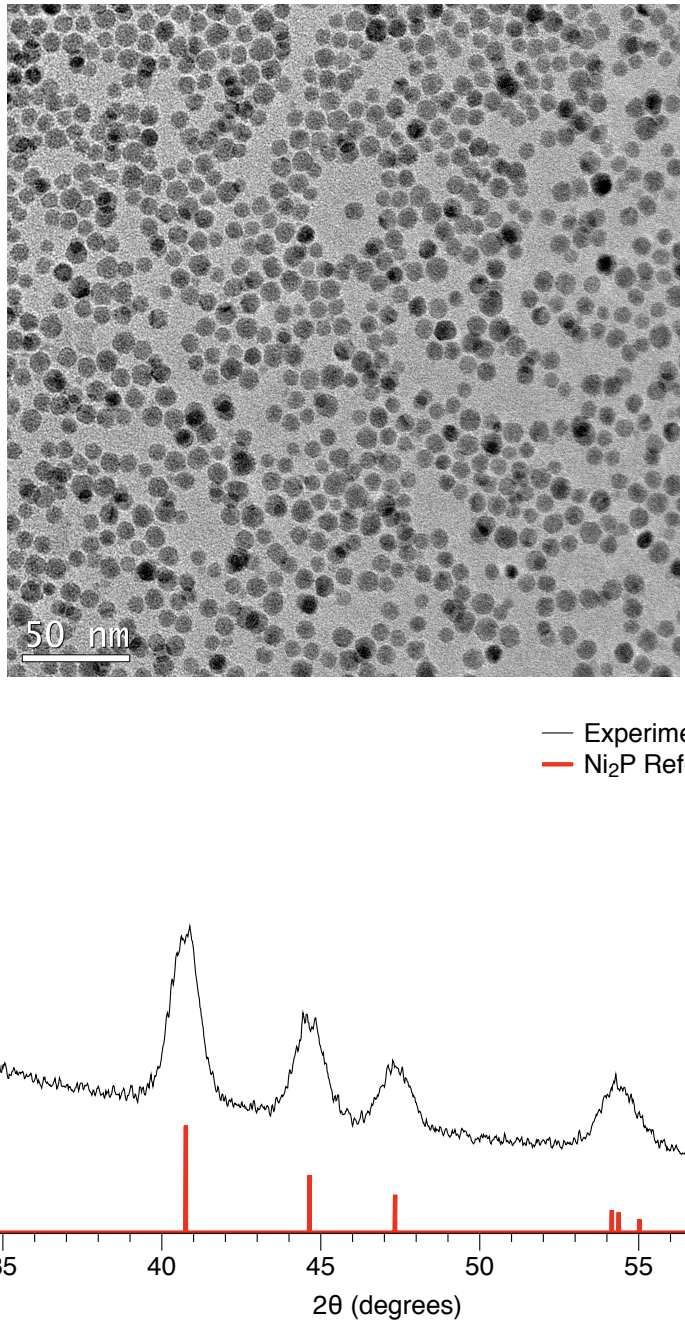


Figure 3.17. TEM of as-synthesized $Ni_2P$ (top) and powder XRD showing phase pure $Ni_2P$ (bottom).

### 3.8.3 *Electrochemical characterization*

Electrochemical measurements were conducted in a custom four-neck cell fitted with a platinum counter electrode (BASi), a Ag wire pseudo reference electrode in a Vycor-fritted compartment (BASi) filled with $TBAPF_6$ and MeCN, and a carbon fiber working electrode. The carbon fiber working electrodes were fabricated from carbon fiber paper (Fuel Cell Store, Spectracarb 2050A 0850). The carbon fiber paper was cut into 1 cm x 3 cm rectangles and a copper wire was attached with a conductive silver epoxy to the electrode material. After curing, the copper wire and silver epoxy were covered with gel epoxy to create a 1 cm x 1 cm working area on the electrode. The backside of the 1 cm x 1 cm working area of the electrode was not covered due to the porosity of the material and epoxy being able to leak onto both sides. The $Ni_2P$ samples were suspended in toluene in a glovebox and dropcasted in 20 μL aliquots onto the working electrodes for electrochemical measurements. The working electrodes were transferred to gas-tight headspace vials with magnetic caps and septa and were brought into a nitrogen filled glovebox for electrochemical measurements.

All electrochemical measurements were performed with a Gamry Interface 1000. The electrolyte solution is typically 0.1-0.2 M $TBAPF_6$ in MeCN. $[HNEt_3][PF_6]$, anilinium [BF4], and [H-DMF][OTf] were used as proton donors in non-aqueous electrolyte solutions. The solutions of Meerwein's reagent were prepared in acetonitrile. When stripping off surface ligands, the electrode was removed from the cell, rinsed with copious amounts of MeCN, dipped in a vial of 0.1 M Meerwein's reagent in 60 s increments, and then rinsed with MeCN before reinsertion into the cell. Linear sweep voltammograms were performed at a scan rate of 5 mV/s. All non-aqueous electrochemical measurements were referenced versus ferrocene.

### 3.8.4 *Characterization methods*

TEM images were collected on an FEI Tecnai G2 F2O microscope. Powder XRD data was collected on a Bruker Microfocus instrument. Powder XRD samples were prepared by drop casting a solution of the as-synthesized $Ni_2P$ onto silicon <001> single crystal wafers. Contact angle measurements were performed on a Kruss DSA100L drop shape analyzer on 3-mercaptopropyltrimethoxysilane treated glass slides.

### 3.8.5 *Preparation of 3-mercaptopropyltrimethoxysilane treated glass slides*

Glass slides were sonicated in solutions of soap, distilled water, acetone, and then isopropyl alcohol in order to clean substrates. After cleaning, the slides were submerged in a 5% v/v MPTS in toluene solution overnight.[31] After treatment, the slides were washed with toluene three times, followed by sonication in a solution of toluene for 5 min. The glass slides were then rinsed and sonicated in an ethanol solution. The slides were dried in an oven at 160 ºC before use. Multi-layer thick films were drop casted to ensure that the contact angle measurements were representative of the film rather than the glass support.

### 3.8.6 *Preparation of $[HNEt_3][PF_6]$*

1 equivalent of triethylammonium chloride was dissolved in water. In a separate container, 1 equivalent of $NaPF_6$ was dissolved in water. The reaction solutions were mixed and a white powder crashed out. The powder was filtered and recrystallized in MeCN three times before drying under vacuum to be used in electrochemical measurements.

### 3.8.7 *Preparation of anilinium [$BF_4$]*

Synthesis was adapted from a previously reported preparation.[32] In a glovebox, 3 g of aniline was dissolved in 5 mL of diethyl ether. 5 g of tetrafluoroboric acid diethyl ether complex was added to the reaction flask dropwise while stirring. **CAUTION:** reaction is extremely exothermic. A gummy white solid precipitated and was collected via filtration. The white solid was dissolved in minimal MeCN, transferred to a new flask, and crashed out with diethyl ether. This solid was collected via filtration and rinsed with copious amounts of diethyl ether before drying under vacuum to be used in electrochemical measurements.

### 3.8.8 *Preparation of [H-DMF][OTf]*

Synthesis was adapted from a previously reported preparation.[9] In a glovebox, 50 mL of dimethylformamide was dissolved in 250 mL of dichloromethane in a 500 mL Schlenk flask. 100 g trifluoromethanesulfonic acid was added dropwise while stirring. **CAUTION:** reaction is extremely exothermic. The reaction was stirred overnight. The solvent was removed under vacuum yielding a white solid which was dried overnight before use in electrochemical measurements.

### 3.8.9 *Preparation of tetrabutylammonium ß-alanine salt*

Synthesis was adapted from a previously reported preparation.[9,10] 1 g of ß-alanine was suspended in ~30 mL water in a 100 mL round bottom flask. 7.3 g of 40% tetrabutylammonium hydroxide solution was added and the reaction solution was heated to 60 ºC for 40 min while stirring. The solvent was removed under vacuum to yield a gummy white solid. The white solid was then suspended in MeCN, which formed a slightly yellow solution with insoluble white solid. The remaining white solid was filtered off and the supernatant was retained. The

supernatant was then dried under vacuum to yield a viscous yellow ionic liquid (tetrabutylammonium ß-alanine salt).

## 3.1 References


(1) Kanicky, J. R.; Shah, D. O. Effect of Degree, Type, and Position of Unsaturation on the pKa of Long-Chain Fatty Acids. *J. Colloid Interface Sci.* **2002**, *256* (1), 201–207.

(2) McCrory, C. C. L.; Jung, S.; Ferrer, I. M.; Chatman, S.; Peters, J. C.; Jaramillo, T. F. Benchmarking Hydrogen Evolving Reaction and Oxygen Evolving Reaction Electrocatalysts for Solar Water Splitting Devices. *J. Am. Chem. Soc.* **2015**, No. 137, 4347–4357.

(3) McCrory, C. C. L.; Jung, S.; Peters, J. C.; Jaramillo, T. F. Benchmarking Heterogeneous Electrocatalysts for the Oxygen Evolution Reaction. *J. Am. Chem. Soc.* **2013**, *135* (45), 16977–16987.

(4) Hoogvliet, J. C.; Dijksma, M.; Kamp, B.; Van Bennekom, W. P. Electrochemical Pretreatment of Polycrystalline Gold Electrodes to Produce a Reproducible Surface Roughness for Self-Assembly: A Study in Phosphate Buffer PH 7.4. *Anal. Chem.* **2000**, *72* (9), 2016–2021.

(5) Wang, Y.; Sun, Y.; Liao, H.; Sun, S.; Li, S.; Ager, J. W.; Xu, Z. J. Activation Effect of Electrochemical Cycling on Gold Nanoparticles towards the Hydrogen Evolution Reaction in Sulfuric Acid. *Electrochim. Acta* **2016**, *209*, 440–447.

(6) Roberts, J. A. S.; Bullock, R. M. Direct Determination of Equilibrium Potentials for Hydrogen Oxidation/Production by Open Circuit Potential Measurements in Acetonitrile. *Inorg. Chem.* **2013**, *52* (7), 3823–3835.

(7) Appel, A. M.; Helm, M. L. Determining the Overpotential for a Molecular Electrocatalyst. *ACS Catal.* **2014**, *4* (2), 630–633.

(8) Fourmond, V.; Jacques, P.-A.; Fontecave, M.; Artero, V. H2 Evolution and Molecular Electrocatalysts: Determination of Overpotentials and Effect of Homoconjugation. *Inorg. Chem.* **2010**, *49* (22), 10338–10347.

(9) McCarthy, B. D.; Martin, D. J.; Rountree, E. S.; Ullman, A. C.; Dempsey, J. L. Electrochemical Reduction of Brønsted Acids by Glassy Carbon in Acetonitrile-Implications for Electrocatalytic Hydrogen Evolution. *Inorg. Chem.* **2014**, *53* (16), 8350–8361.

(10) Favier, I.; Duñach, E. New Protic Salts of Aprotic Polar Solvents. *Tetrahedron Lett.* **2004**, *45* (17), 3393–3395.

(11) Xiao, P.; Sk, M. A.; Thia, L.; Ge, X.; Lim, R. J.; Wang, J.-Y.; Lim, K. H.; Wang, X. Molybdenum Phosphide as an Efficient Electrocatalyst for the Hydrogen Evolution Reaction. *Energy Environ. Sci.* **2014**, *7* (8), 2624–2629.

(12) Yang, X.; Nash, J.; Oliveira, N.; Yan, Y.; Xu, B. Understanding the PH Dependence of Underpotential Deposited Hydrogen on Platinum. *Angew. Chemie Int. Ed.* **2019**, 2–8.

(13) Ledezma-Yanez, I.; Wallace, W. D. Z.; Sebastián-Pascual, P.; Climent, V.; Feliu, J. M.; Koper, M. T. M. Interfacial Water Reorganization as a PH-Dependent Descriptor of the Hydrogen Evolution Rate on Platinum Electrodes. *Nat. Energy* **2017**, *2* (4), 1–7.

(14) Lamoureux, P. S.; Singh, A. R.; Chan, K. PH Effects on Hydrogen Evolution and Oxidation over Pt(111): Insights from First-Principles. *ACS Catal.* **2019**, *9* (111), 6194–6201.
(15) Wiedner, E. S.; Brown, H. J. S.; Helm, M. L. Kinetic Analysis of Competitive Electrocatalytic Pathways: New Insights into Hydrogen Production with Nickel Electrocatalysts. *J. Am. Chem. Soc.* **2016**, *138* (2), 604–616.
(16) Kumar, B.; Llorente, M.; Froehlich, J.; Dang, T.; Sathrum, A.; Kubiak, C. P. Photochemical and Photoelectrochemical Reduction of CO2. *Annu. Rev. Phys. Chem.* **2012**, *63*, 541–569.
(17) DuBois, D. L. Development of Molecular Electrocatalysts for Energy Storage. *Inorg. Chem.* **2014**, *53* (8), 3935–3960.
(18) Pool, D. H.; Stewart, M. P.; O'Hagan, M.; Shaw, W. J.; Roberts, J. A. S.; Bullock, R. M.; DuBois, D. L. Acidic Ionic Liquid/Water Solution as Both Medium and Proton Source for Electrocatalytic H2 Evolution by [Ni(P2N2) 2]2+ Complexes. *Proc. Natl. Acad. Sci. U. S. A.* **2012**, *109* (39), 15634–15639.
(19) Galan, B. R.; o ffel, J.; Linehan, J. C.; Seu, C. S.; Appel, A. M.; Roberts, J. a S.; Helm, M. L.; Kilgore, U. J.; Yang, J. Y.; DuBois, D. L.; et al. Electrocatalytic Oxidation of Formate by [Ni(P(R)2N(R')2)2(CH3CN)]2+ Complexes. *J. Am. Chem. Soc.* **2011**, *133* (32), 12767–12779.
(20) Machan, C. W.; Sampson, M. D.; Chabolla, S. a; Dang, T.; Kubiak, P. Developing a Mechanistic Understanding of Molecular Electrocatalysts for CO 2 Reduction Using Infrared Spectroelectrochemistry. **2014**, 2–11.
(21) Nimlos, M. R.; Chang, C. H.; Curtis, C. J.; Miedaner, A.; Pilath, H. M.; DuBois, D. L. Calculated Hydride Donor Abilities of Five-Coordinate Transition Metal Hydrides [HM(Diphosphine)2]+ (M = Ni, Pd, Pt) as a Function of the Bite Angle and Twist Angle of Diphosphine Ligands. *Organometallics* **2008**, *27* (12), 2715–2722.
(22) Seu, C. S.; Ung, D.; Doud, M. D.; Moore, C. E.; Rheingold, A. L.; Kubiak, C. P. Synthesis, Structural, and Electrocatalytic Reduction Studies of [Pd(P2N2)2]2+ Complexes. *Organometallics* **2013**, *32* (16), 4556–4563.
(23) Pegis, M. L.; Wise, C. F.; Martin, D. J.; Mayer, J. M. Oxygen Reduction by Homogeneous Molecular Catalysts and Electrocatalysts. *Chem. Rev.* **2018**, *118* (5), 2340–2391.
(24) Gao, W.; Gou, W.; Zhou, X.; Ho, J. C.; Ma, Y.; Qu, Y. Amine-Modulated/Engineered Interfaces of NiMo Electrocatalysts for Improved Hydrogen Evolution Reaction in Alkaline Solutions. *ACS Appl. Mater. Interfaces* **2018**, *10*, 1728–1733.
(25) Xu, G. R.; Bai, J.; Yao, L.; Xue, Q.; Jiang, J. X.; Zeng, J. H.; Chen, Y.; Lee, J. M. Polyallylamine-Functionalized Platinum Tripods: Enhancement of Hydrogen Evolution Reaction by Proton Carriers. *ACS Catal.* **2017**, *7* (1), 452–458.
(26) Li, Y.; Zhao, C. Enhancing Water Oxidation Catalysis on a Synergistic Phosphorylated NiFe Hydroxide by Adjusting Catalyst Wettability. *ACS Catal.* **2017**, *7* (4), 2535–2541.
(27) Pankhurst, J. R.; Guntern, Y. T.; Mensi, M.; Buonsanti, R. Molecular Tunability of Surface-Functionalized Metal Nanocrystals for Selective Electrochemical CO 2 Reduction. *Chem. Sci.* **2019**, No. ii.
(28) Rigsby, M. L.; Wasylenko, D. J.; Pegis, M. L.; Mayer, J. M. Medium Effects Are as Important as Catalyst Design for Selectivity in Electrocatalytic Oxygen Reduction by Iron-Porphyrin Complexes. *J. Am. Chem. Soc.* **2015**, *137* (13), 4296–4299.
(29) Kibsgaard, J.; Tsai, C.; Chan, K.; Benck, J. D.; Nørskov, J. K.; Abild-Pedersen, F.;

Jaramillo, T. F. Designing an Improved Transition Metal Phosphide Catalyst for Hydrogen Evolution Using Experimental and Theoretical Trends. *Energy Environ. Sci.* **2015**, *8* (10), 3022–3029.

(30) Gardner, J. R.; Woods, R. The Hydrophilic Nature of Gold and Platinum. *J. Electroanal. Chem.* **1977**, *81* (2), 285–290.

(31) Muthuswamy, E.; Savithra, G. H. L.; Brock, S. L. Synthetic Levers Enabling Independent Control of Phase, Size, and Morphology in Nickel Phosphide Nanoparticles. *ACS Nano* **2011**, *5* (3), 2402–2411.

(32) Pallavicini, P.; Dacarro, G.; Galli, M.; Patrini, M. Spectroscopic Evaluation of Surface Functionalization Efficiency in the Preparation of Mercaptopropyltrimethoxysilane Self-Assembled Monolayers on Glass. *J. Colloid Interface Sci.* **2009**, *332* (2), 432–438.

# APPENDIX A: BENCHMARKING ELECTROCATALYTIC TRANSITION METAL PHOSPHIDES SYNTHESIZED VIA AMINOPHOSPHINE PRECURSORS

Note: Significant portions of the following chapter have previously been published.[1] This work was done in collaboration with my colleagues Beth Mundy and Nathan Lai in the Cossairt lab, as well as Dr. Evan Jahrman in Professor Gerald Seidler's group in the Department of Physics.

Traditional colloidal syntheses for electrocatalytic transition metal phosphides are carried out using a metal precursor, phosphorus precursor, and reducing agent. Often times these syntheses require two steps, the first to form a metal nanoparticle which is then isolated and purified, and the second to incorporate phosphorus via a Kirkendall mechanism.[2–6] The phosphidation reaction is typically performed at temperatures >300 ºC for extended durations. These harsh synthetic conditions are due to the low reactivity of the most common phosphorus precursor, trioctylphosphine (TOP). Transition metal phosphides require the presence of a $P^{3-}$ precursor, but most phosphorus precursors are in the 3+ oxidation state. Heating the trioctylphosphine precursor to >300 ºC converts the TOP through a series of β-hydride elimination reactions to $PH_3$ gas, which is an extremely reactive $P^{3-}$ precursor. While this method is effective in producing phase-pure TMPs, they require harsh reaction conditions and can often have low yields due to the reaction requiring the isolation of a metal nanoparticle intermediate.

Recent work has focused on developing new synthetic methods that can be done in one step with milder reaction conditions. Aminophosphines have been shown as a promising phosphorus precursor for the synthesis of TMPs. In a typical synthesis, a metal halide salt is dissolved in a long chain primary amine, degassed, heated to 200-250 ºC, and tris-

diethylaminophosphine is injected and the nanocrystals are allowed to form over a period of time.

This synthetic method developed has been shown by our group to be an effective strategy to produce phase-pure $Co_2P$, CoP, and $Ni_2P$ which are all known to be electrocatalytically competent for HER when synthesized via the traditional TOP method. The aminophosphine synthesized $Co_2P$, CoP, and $Ni_2P$ were drop casted on carbon fiber electrodes and the surface ligands were removed through thermal annealing as well as alkylation with triethyloxonium tetrafluoroborate. Alkylation was shown to have similar overpotentials to thermal treatments, with the exception of $Ni_2P$, which showed significantly improved activity after thermal treatments when compared to the alkylation. These results illustrate that aminophosphine precursors are effective at producing phase-pure, electrocatalytically active TMPs in a one-step synthesis at milder reaction temperatures.

Table A.1. Overpotentials of TMPs with different methods of ligand removal

| Material | $\eta_{10mA/cm2}$ annealed on CF | $\eta_{10mA/cm2}$ Meerwein's treated on CF |
|---|---|---|
| CoP | 315 mV | 314 mV |
| $Co_2P$ | 169 mV | 160 mV |
| $Ni_2P$ | 147 mV | 246 mV |

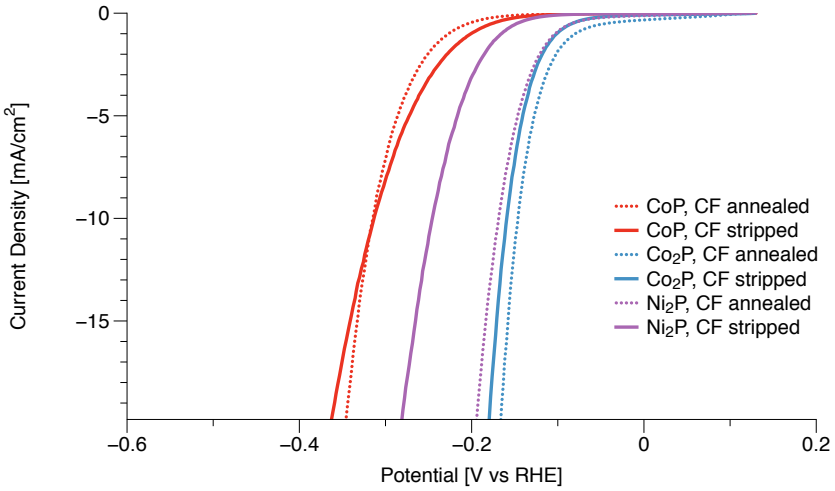


Figure A.1. LSVs of the range of aminophosphine synthesized TMPs with different methods of ligand removal on carbon fiber working electrodes.

## References


(1) Mundy, M. E.; Ung, D.; Lai, N. L.; Jahrman, E. P.; Seidler, G. T.; Cossairt, B. M. Aminophosphines as Versatile Precursors for the Synthesis of Metal Phosphide Nanocrystals. *Chem. Mater.* **2018**, *30* (15), 5373–5379.

(2) Ha, D.-H.; Moreau, L. M.; Bealing, C. R.; Zhang, H.; Hennig, R. G.; Robinson, R. D. The Structural Evolution and Diffusion during the Chemical Transformation from Cobalt to Cobalt Phosphide Nanoparticles. *J. Mater. Chem.* **2011**, *21* (31), 11498–11510.

(3) Sun, M.; Liu, H.; Qu, J.; Li, J. Earth-Rich Transition Metal Phosphide for Energy Conversion and Storage. *Adv. Energy Mater.* **2016**, *6* (13), 1–34.

(4) Saadi, F. H.; Carim, A. I.; Verlage, E.; Hemminger, J. C.; Lewis, N. S.; Soriaga, M. P. CoP as an Acid-Stable Active Electrocatalyst for the Hydrogen-Evolution Reaction: Electrochemical Synthesis, Interfacial Characterization and Performance Evaluation. *J. Phys. Chem. C* **2014**, *118* (50), 29294–29300.

(5) Callejas, J. F.; Read, C. G.; Popczun, E. J.; McEnaney, J. M.; Schaak, R. E. Nanostructured Co2P Electrocatalyst for the Hydrogen Evolution Reaction and Direct Comparison with Morphologically Equivalent CoP. *Chem. Mater.* **2015**, *27* (10), 3769–3774.

(6) Pan, Y.; Liu, Y.; Zhao, J.; Yang, K.; Liang, J.; Liu, D.; Hu, W.; Liu, D.; Liu, Y.; Liu, C. Monodispersed Nickel Phosphide Nanocrystals with Different Phases: Synthesis, Characterization and Electrocatalytic Properties for Hydrogen Evolution. *J. Mater. Chem. A* **2015**, *3* (4), 1656–1665.

# VITA

David Ung was born and raised in Los Angeles, California. His parents immigrated to the United States from Cambodia and raised David, his older sister, and his older brother in the Echo Park neighborhood of Los Angeles. David was science-averse while growing up and originally wanted to attend film school for college. He gained an appreciation for science after taking a chemistry class in his junior year of high school, and ended up receiving his chemistry degree at the University of California, San Diego. He then moved to Seattle to pursue a Ph.D. in chemistry at the University of Washington. In his free time, David enjoys photography, eating food around the world with his siblings, riding bicycles, and is a professional yo-yo player. David is the first to earn a Ph.D. in his family.